TDP-43 loss of function inhibits endosomal trafficking and alters trophic signaling in neurons

Benjamin M Schwenk[1,2], Hannelore Hartmann[1], Alperen Serdaroglu[1,3], Martin H Schludi[1,2], Daniel Hornburg[4], Felix Meissner[4], Denise Orozco[1], Alessio Colombo[1], Sabina Tahirovic[1], Meike Michaelsen[1], Franziska Schreiber[1], Simone Haupt[5], Michael Peitz[6,7], Oliver Brüstle[6], Clemens Küpper[2,8], Thomas Klopstock[1,2,8], Markus Otto[9], Albert C Ludolph[9], Thomas Arzberger[1,10,11], Peer-Hendrik Kuhn[1,3,12] & Dieter Edbauer[1,2,13,*]

Abstract

Nuclear clearance of TDP-43 into cytoplasmic aggregates is a key driver of neurodegeneration in amyotrophic lateral sclerosis (ALS) and frontotemporal lobar degeneration (FTLD), but the mechanisms are unclear. Here, we show that TDP-43 knockdown specifically reduces the number and motility of RAB11-positive recycling endosomes in dendrites, while TDP-43 overexpression has the opposite effect. This is associated with delayed transferrin recycling in TDP-43-knockdown neurons and decreased β2-transferrin levels in patient CSF. Whole proteome quantification identified the upregulation of the ESCRT component VPS4B upon TDP-43 knockdown in neurons. Luciferase reporter assays and chromatin immunoprecipitation suggest that TDP-43 represses VPS4B transcription. Preventing VPS4B upregulation or expression of its functional antagonist ALIX restores trafficking of recycling endosomes. Proteomic analysis revealed the broad reduction in surface expression of key receptors upon TDP-43 knockdown, including ErbB4, the neuregulin 1 receptor. TDP-43 knockdown delays the surface delivery of ErbB4. ErbB4 overexpression, but not neuregulin 1 stimulation, prevents dendrite loss upon TDP-43 knockdown. Thus, impaired recycling of ErbB4 and other receptors to the cell surface may contribute to TDP-43-induced neurodegeneration by blocking trophic signaling.

Keywords ALS; ErbB4; FTLD; recycling endosomes; TDP-43
Subject Categories Membrane & Intracellular Transport; Neuroscience

Introduction

TDP-43 is a DNA/RNA-binding protein that represses transcription and regulates RNA metabolism predominantly in the nucleus. Cytoplasmic TDP-43 inclusions are pathological hallmarks of most ALS and FTLD cases, and their regional distribution correlates remarkably well with neurodegeneration (Geser *et al*, 2009b; Ling *et al*, 2013). Degeneration of the frontal and temporal lobe in FTLD causes behavioral changes as well as speech and language impairment. Degeneration of upper and lower motoneurons in ALS leads to progressive paralysis (Ferrari *et al*, 2011). Both diseases often overlap clinically and share a strong genetic component with several genes linked to both ALS and FTLD (Ling *et al*, 2013). Pathogenic mutations in TDP-43 are found in 1–3% of familial ALS cases and seem to mainly promote aggregation without the obvious deleterious effects on the function of the soluble TDP-43 (Kabashi *et al*, 2008; Sreedharan *et al*, 2008; Johnson *et al*, 2009). Intriguingly, TDP-43 inclusions are found in about 90% of ALS and 45% of FTLD cases (Geser *et al*, 2009a; Mackenzie *et al*, 2010), including most sporadic cases without known causal mutation. Hippocampal TDP-43 inclusions are also common in Alzheimer cases, where they are associated with cognitive decline (Davidson *et al*, 2011).

1   German Center for Neurodegenerative Diseases (DZNE), Munich, Germany
2   Munich Cluster of Systems Neurology (SyNergy), Munich, Germany
3   Institute for Advanced Study, Technische Universität München, München, Germany
4   Max Planck Institute of Biochemistry, Martinsried, Germany
5   LIFE & BRAIN GmbH, Bonn, Germany
6   Institute of Reconstructive Neurobiology, University of Bonn, Bonn, Germany
7   German Center for Neurodegenerative Diseases (DZNE), Bonn, Germany
8   Department of Neurology, Friedrich-Baur-Institute, LMU Munich, Munich, Germany
9   Department of Neurology, University of Ulm, Ulm, Germany
10   Center for Neuropathology and Prion Research, LMU Munich, Munich, Germany
11   Department of Psychiatry and Psychotherapy, LMU Munich, Munich, Germany
12   Institut für Allgemeine Pathologie, Klinikum rechts der Isar der Technischen Universität München, München, Germany
13   Institute for Metabolic Biochemistry, LMU Munich, Munich, Germany
   *Corresponding author. Tel: +49 89 4400 46510; E-mail: dieter.edbauer@dzne.de

Most cells with TDP-43 aggregates show nearly complete clearance of nuclear TDP-43, suggesting a combination of loss of nuclear function and gain of toxic function. Although the physiological role of TDP-43 is incompletely understood, many putative RNA targets have been identified, which are essential for neuronal function and survival (Buratti *et al*, 2013). Despite the mostly nuclear localization of TDP-43, a smaller cytoplasmic TDP-43 fraction has been implicated in axonal trafficking of mRNA transport granules (Alami *et al*, 2014). Overexpression of wild-type or mutant TDP-43 causes neuron loss, and complete TDP-43 knockout is lethal in mice (Gendron & Petrucelli, 2011). Selective neurodegeneration in conditional knockout mice suggests that cell-autonomous effects govern the toxicity (Wu *et al*, 2012). As homozygous knockout mice die in an early embryonic stage, TDP-43 is thought to have a crucial role in fundamental cellular pathways (Gendron & Petrucelli, 2011). Despite a large number of RNAs potentially binding to TDP-43, the major cause of neurotoxicity upon knockout is still unclear (Polymenidou *et al*, 2011; Tollervey *et al*, 2011).

Several proteins genetically linked to TDP-43 pathology play important roles in the endolysosomal pathway, which consists of different vesicle pools distinguishable by specific RAB-GTPases that regulate vesicle transport. The key compartments are RAB5-positive early endosomes, RAB11-positive recycling endosomes, and RAB7-positive late endosomes/lysosomes (Schwartz *et al*, 2007). In addition, RAB4-positive endosomes allow faster recycling to the plasma membrane by skipping the endosomal recycling compartment critical for RAB11-dependent recycling (Sonnichsen *et al*, 2000; Maxfield & McGraw, 2004). This network governs the sorting of internalized cell surface proteins either for lysosomal degradation or for recycling to the plasma membrane and thus controls cellular signaling. CHMP2B is part of the endosomal sorting complexes required for transport (ESCRT) that mediates membrane remodeling, and rare FTLD-causing mutations in *CHMP2B* disrupt endocytic trafficking and fusion with lysosomes (Skibinski *et al*, 2005; Urwin *et al*, 2010). The ESCRT complex consists of four cytosolic protein complexes (ESCRT-0, -I, -II, and -III) that regulate together with ESCRT accessory factors, for example, VPS4 and ALIX, membranes bending and budding. This machinery is crucial for cellular processes such as vesicle sorting, MVB biogenesis, virus budding, and cellular abscission (Tu *et al*, 2011). Moreover, the FTLD-TDP risk factor TMEM106B controls trafficking of RAB7-positive lysosomes in dendrites (Schwenk *et al*, 2014; Stagi *et al*, 2014). While GRN haploinsufficiency is a common cause of FTLD with TDP-43 pathology, rare patients with homozygous loss of GRN suffer from the lysosomal storage disease neuronal ceroid lipofuscinosis (Smith *et al*, 2012). Vice versa, patients with neuronal ceroid lipofuscinosis show signs of TDP-43 pathology (Gotzl *et al*, 2014). Pathogenic mutations in TBK1 and OPTN suggest that altered autophagy may trigger ALS and FTLD with TDP-43 pathology (Cirulli *et al*, 2015; Freischmidt *et al*, 2015). These chronic defects in protein degradation eventually lead to the aggregation of TDP-43. Here, we asked how loss of TDP-43 harms neuron function using live imaging of endosomes in primary neurons transfected with different fluorescently labeled vesicular markers and identified new TDP-43 targets by whole proteome quantification. We validated key findings in patient-derived material. This uncovered an unexpected link of TDP-43 with another ALS-associated gene, ErbB4.

Results

## Loss of TDP-43 in primary neurons reduces the number and motility of recycling endosomes

To analyze the role of TDP-43 on trafficking in the endolysosomal compartment in primary neurons, we generated specific shRNA constructs. Knockdown efficiency was confirmed on mRNA and protein levels in rat primary hippocampal neurons transduced with a lentivirus expressing either the TDP-43 shRNA (shTDP) or a control shRNA (shCtrl, targeting firefly luciferase) (Appendix Fig S1A–C). Moreover, transfecting hippocampal neurons with the TDP-43 shRNA reduced TDP-43 levels detected by immunofluorescence within three days (Appendix Fig S1D).

Next, we cotransfected hippocampal neurons at six days *in vitro* with shTDP or shCtrl together with GFP-tagged vesicle markers (RAB4, RAB5, RAB7, RAB11) to analyze how the loss of TDP-43 affects endolysosomal trafficking (Figs 1, EV1, and EV2). After three days of knockdown (DIV6+3), we analyzed organelle transport in dendrites by live cell imaging of the transfected neurons and subsequently transformed the images into kymographs (path-time diagrams of organelle transport) to visualize the movement pattern. We quantified the total number and the number of moving and stationary GFP-labeled vesicles from these kymographs. Among the tested vesicle pools, TDP-43 knockdown had the strongest effect on RAB11-positive recycling endosomes. The dendritic motility of GFP-RAB11-labeled endosomes was strongly reduced in TDP-43-knockdown neurons compared to controls (Fig 1A–C). While the number of stationary recycling endosomes was unchanged, the number of mobile recycling endosomes was reduced to half upon TDP-43 knockdown (Fig 1B) resulting in an overall loss of RAB11-positive recycling endosomes (Fig 1C). We found no colocalization of TDP-43 and GFP-RAB11 in primary neurons (Appendix Fig S1E), suggesting that TDP-43 regulates a key protein in the recycling pathway. The effects of TDP-43 on recycling endosome motility were fully confirmed using a second shRNA (Appendix Fig S2A–D). In contrast, knockdown of TMEM106B, linked to TDP-43 pathology and lysosomal trafficking (Schwenk *et al*, 2014; Stagi *et al*, 2014), did not affect GFP-RAB11-labeled recycling endosomes (Appendix Fig S2E–H). Thus, TDP-43, but not TMEM106B, is required to maintain the proper number and motility of RAB11-positive recycling endosomes in dendrites.

To test whether this phenotype is conserved in humans and thus may be relevant for FTLD/ALS, we additionally analyzed trafficking of recycling endosomes upon TDP-43 knockdown in human neurons. We transduced iPSC-derived human neurons with a lentivirus expressing a shRNA targeting human TDP-43 or a control shRNA (Fig 1D). Similar to rat neurons, GFP-RAB11-labeled recycling endosomes were less abundant and less motile (Fig 1E–G). Hence, the role of TDP-43 in promoting the motility of recycling endosomes is conserved between rats and humans.

Trafficking of other organelles remains intact in TDP-43-knockdown neurons

To rule out an overall transport defect upon TDP-43 knockdown, we analyzed the trafficking of mitochondria labeled by cotransfection
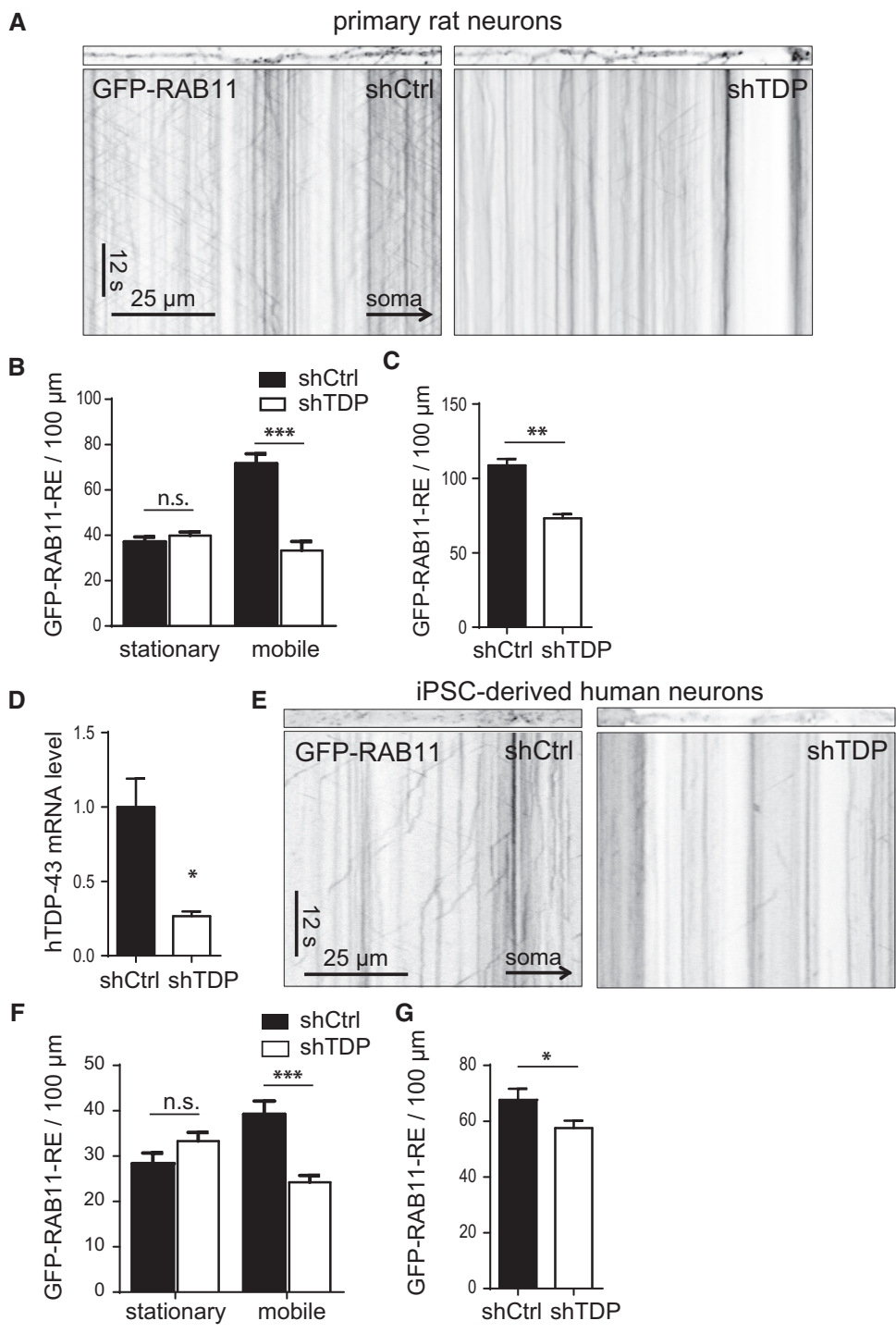
Figure 1. TDP-43 knockdown in primary rat and iPSC-derived human neurons inhibits trafficking of recycling endosomes in dendrites.

A Primary hippocampal neurons (DIV6+3) were transfected with shRNA targeting TDP-43 (shTDP) or control (shCtrl) together with GFP-RAB11 to visualize trafficking of recycling endosomes (RE). At least four dendrite segments per neuron were live-imaged at 5 Hz for 1 min to analyze recycling endosome transport. Representative dendrite segments and kymographs of GFP-RAB11 vesicle movement.

B, C Quantitative analysis of vesicle motility (B) and the total number (C) from kymographs in (A).

D iPSC-derived human neurons were transduced 7 days after thawing for 3 days with shRNA targeting human TDP-43 (shTDP) or control (shCtrl). TDP-43 levels were analyzed by quantitative RT-PCR. Expression was normalized to the housekeeping genes YWHAZ and PGK1.

E iPSC-derived human neurons (DIV7+3) were transduced with shTDP or shCtrl and GFP-RAB11 and at least three dendrite segments per neuron analyzed as in (A). Representative dendrite segments and kymographs of GFP-RAB11 vesicle movement.

F, G Quantitative analysis of vesicle motility (F) and number (G) from kymographs in (E).

Data information: Mean ± s.e.m., $n = 3$, unpaired two-tailed t-test: *$P < 0.05$, **$P < 0.01$, ***$P < 0.001$.

with mito-GFP in rat primary neurons. Mitochondria number and motility were undistinguishable in the dendrites of neurons transfected with TDP-43 or control shRNA (Fig EV1A–C), suggesting that the loss of TDP-43 has no general effect on microtubule-mediated transport.

Trafficking of the other endosomal populations was also not affected by TDP-43 knockdown as analyzed by live cell imaging of GFP-RAB5-labeled (early endosomes) and GFP-RAB4-labeled (endosomes directly recycling to the plasma membrane) vesicles (Fig EV1D–I). However, TDP-43 knockdown slightly promoted the motility of GFP-RAB7-labeled lysosomes (Fig EV2A and B). In contrast to the retrograde-specific increase in lysosomal motility upon TMEM106B knockdown (Schwenk *et al*, 2014), TDP-43 knockdown increased both anterograde and retrograde lysosomal trafficking equally (Fig EV2C). The overall number of GFP-RAB7-labeled lysosomes remained unchanged upon TDP-43 knockdown (Fig EV2D).

Thus, TDP-43 loss specifically inhibits the motility of RAB11-positive recycling endosomes in the dendrites potentially in favor of lysosomal motility without impairing the transport of RAB5-positive early endosomes, RAB4-positive fast recycling endosomes or mitochondria.

TDP-43 knockdown inhibits transferrin recycling

To elucidate the functional consequences of impaired trafficking of recycling endosomes, we analyzed the constitutive uptake and recycling of the prototypical cargo transferrin through the endocytic pathway. After receptor binding, the receptor–ligand complex is endocytosed via clathrin-coated vesicles and transported to the early/sorting endosome. Unlike many other ligands, transferrin does not dissociate from its receptor to terminate signaling, but the whole complex is transferred back to the plasma membrane mainly via the ERC and RAB11-positive recycling endosomes (Sonnichsen *et al*, 2000). We quantified transferrin recycling by measuring the amount of exogenously added fluorescently labeled transferrin in the neurons directly after endocytosis and 20 or 60 min afterward. Control shRNA-transduced rat neurons released 40% of the endocytosed transferrin within 20 min and 60% within 60 min (Fig 2A and B). In contrast, TDP-43-knockdown neurons initially took up the same amount of labeled transferrin, but released about 30% less after 20 and 60 min, indicating that recycling to the plasma membrane is delayed.

To corroborate this finding in patient material, we quantified the transferrin level in the CSF of 55 sporadic ALS patients and 65 controls. To exclude the possible confounds of altered systemic iron metabolism (Nadjar *et al*, 2012) as much as possible, we focused our analysis on the CSF-specific β2-transferrin. Consistent with normal endocytosis but reduced recycling seen in our neuronal model, the ALS patients had lower β2-transferrin levels in CSF than healthy age-matched controls (Fig 2C). A smaller reduction was seen in patients with FTD-ALS (12 patients) and behavioral variant FTD (16 patients), which likely suffer from TDP-43 pathology, although this did not reach statistical significance due to the smaller cohort size.

To confirm that the reduced transport and recycling contributed to the elevated intracellular transferrin levels in the neurons and decreased levels in the extracellular CSF, we analyzed the

motility of transferrin-containing vesicles by live cell imaging. We again added Alexa-labeled transferrin to the neurons and imaged 20 min after endocytosis, when most of endocytosed fluorescent transferrin is expected to have reached the endosomal recycling compartment (Sonnichsen *et al*, 2000). Importantly, labeled transferrin was significantly less mobile in shTDP-transfected neurons than in controls (Fig 2D–F), consistent with the results using GFP-RAB11 transfection (compare Fig 1).

Thus, TDP-43 loss of function impairs dendritic trafficking of recycling endosomes. Evidence for impaired recycling activity is found in rat and human neurons and CSF from ALS patients.

## Overexpression of nuclear, but not cytoplasmic, TDP-43 enhances recycling endosome transport

Next, we asked whether overexpression of wild-type TDP-43 or a mutant lacking the nuclear localization signal (ΔNLS) would promote recycling endosome motility (Fig 3A). Neurons transfected with wild-type TDP-43 showed a higher number of GFP-RAB11-positive recycling endosomes compared to vector-transfected cells, which was exclusively due to an increase in the number of mobile GFP-RAB11-positive vesicles (Fig 3B–D). In contrast, the predominantly cytoplasmic ΔNLS mutant did not affect the number and motility of recycling endosomes. The opposite effects of TDP-43 knockdown and overexpression on recycling endosome motility and abundance further support the specificity of these findings (compare Figs 1 and 3) and suggest that they are mediated by nuclear TDP-43 rather than the smaller cytoplasmic fraction.

To further address whether the loss of nuclear TDP-43 mediates the effects of TDP-43 knockdown, we performed rescue experiments using TDP-43 wild type and ΔNLS. Remarkably, coexpression of wild-type, but not mutant, TDP-43 together with TDP-43 shRNA partially restored the number and motility of GFP-RAB11-labeled recycling endosomes (Fig EV3). In summary, these data indicate that nuclear TDP-43 promotes recycling endosome motility by controlling the expression or splicing of a key regulatory factor in this pathway.

TDP-43 represses transcription of the ESCRT-III accessory protein VPS4B

To elucidate how TDP-43 might regulate recycling endosome trafficking, we performed a quantitative whole proteome analysis in cortical neurons upon lentiviral TDP-43 knockdown or control (DIV2+7) using a label-free LC-MS/MS pipeline (Hornburg *et al*, 2014) (Fig 4A). We observed an upregulation of proteins involved in lipid metabolism and a strong downregulation of proteins annotated for neuron projection, synapse, and various transport processes upon TDP-43 knockdown (Fig 4B and Table EV1). Comparing 5,077 quantified proteins, 63 were changed at least threefold ($\log_2$ cutoff 1.58; Table EV1). However, the overall changes in protein expression were modest despite the large number of putative TDP-43 target genes. Among the affected proteins, VPS4B (vacuolar protein sorting 4 homolog B) was one of the strongest upregulated (3.8-fold) upon TDP-43 knockdown. VPS4B directly binds to the ALS/FTLD gene CHMP2B to disassemble the ESCRT complex and has been
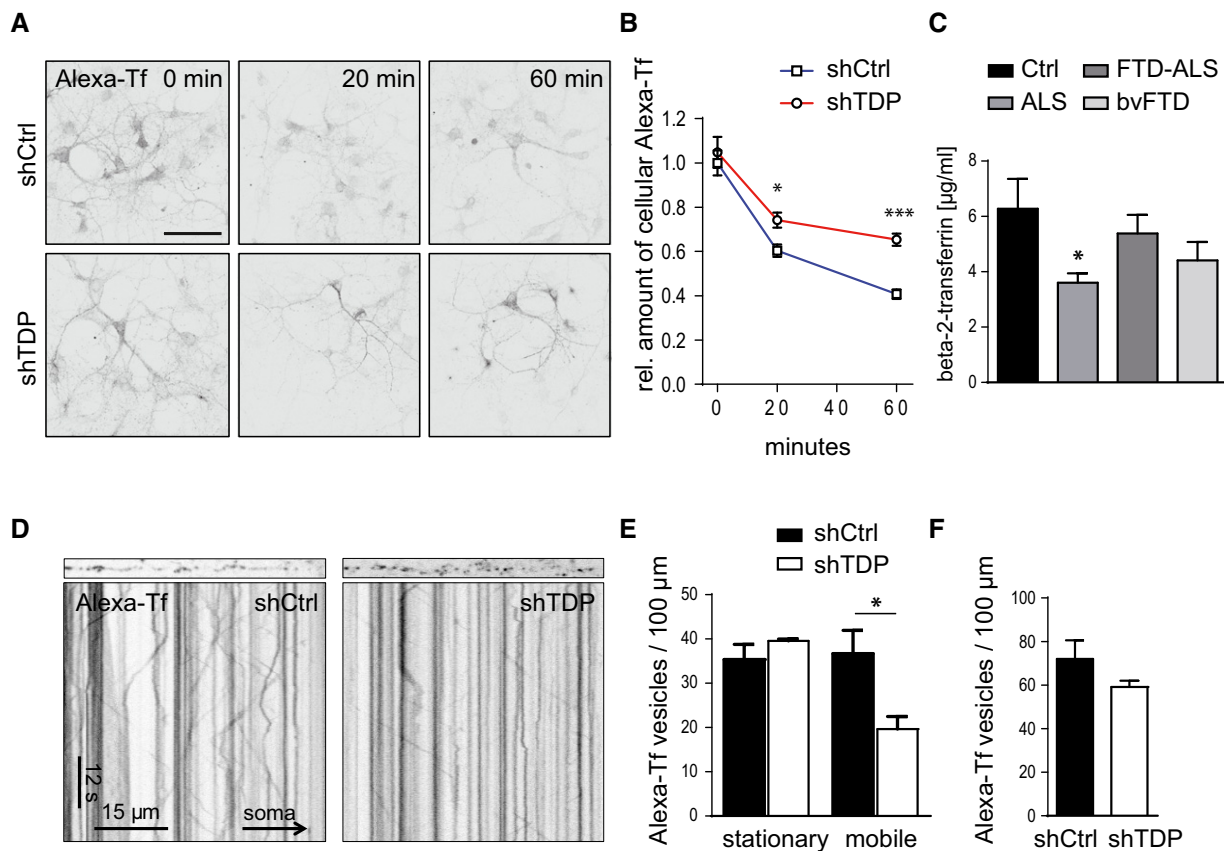
Figure 2. TDP-43 knockdown in primary neurons inhibits transferrin recycling.

A   Primary hippocampal neurons (DIV6+4) were transduced with shRNA targeting TDP-43 or a control together with tagRFP (not depicted). Representative images of neurons subjected to Alexa-transferrin (Alexa-Tf) for 20 min (pulse) and chased for 0, 20, or 60 min in complete media. Scale bar represents 100 μm.

B   Quantification of labeled cellular Alexa-Tf normalized to cell area (using tagRFP) after chase period. At least ten images per condition were analyzed per experiment in three independent experiments.

C   ELISA measurement of β2-transferrin in CSF of control subjects (*n* = 65) and sporadic ALS patients (*n* = 55), FTD-ALS patients (*n* = 12), and behavioral variant FTD patients (bvFTD, *n* = 16).

D   Primary hippocampal neurons (DIV6+3) were transfected with shTDP or shCtrl and GFP as transfection marker. After 3 days, the neurons were subjected to Alexa-Tf for 20 min and intracellular Alexa-Tf movement was imaged as in Fig 1 afterward.

E, F   Quantitative analysis of Alexa-Tf movement (E) and vesicle number (F) from kymographs. *n* = 3.

Data information: Mean ± s.e.m., unpaired, two-tailed *t*-test (E, F), Mann–Whitney *U*-test with Bonferroni's post-test (B) or one-way ANOVA with Dunnet's post-test (C): *$P < 0.05$, ***$P < 0.001$.

implicated in endosomal sorting and transport (Stuchell-Brereton *et al*, 2007; Du *et al*, 2013). In independent validations experiments, both VPS4B mRNA and protein levels were about twofold increased upon lentiviral knockdown of TDP-43 compared to controls (Fig 4C–E). Transfection of TDP-43 shRNA confirmed an increased VPS4B protein expression also on a single-cell level (Fig 4F). Moreover, lentiviral TDP-43 knockdown increased VPS4B levels also in human neurons (Fig 4G), indicating that TDP-43 controls recycling endosome trafficking in rat and human neurons through a conserved mechanism.

To test whether TDP-43 affects VPS4B transcription, we generated a reporter construct containing the 1,000-bp region upstream of the transcriptional start site of VPS4B upstream of luciferase (Fig 5A). We transfected HEK293 cells with either TDP-43 knockdown or overexpression constructs or the respective controls together with the VPS4B reporter construct and

analyzed luciferase expression. While TDP-43 knockdown caused an almost threefold activation of the VPS4B promoter, TDP-43 overexpression significant inhibited VPS4B promoter activity (Fig 5B).

Moreover, we performed chromatin immunoprecipitation to investigate whether TDP-43 directly binds to the VPS4B promoter. To this end, we immunoprecipitated TDP-43 from crosslinked and sheared chromatin preparations of rat cortical neurons. Binding of endogenous TDP-43 to the VPS4B locus was tested using eight PCR amplicons (~200 bp each) covering the promoter region used for the luciferase reporter. Consistent with the known binding preference of TDP-43, we detected binding of TDP-43 to a GT-rich region in the VPS4B promoter (Fig 5C). Moreover, we could confirm the binding of endogenous TDP-43 to a corresponding GT-rich region in the human VPS4B promoter in HEK293 cells and human brain tissue (Fig 5C). Quantification of ChIP assays confirmed a significant
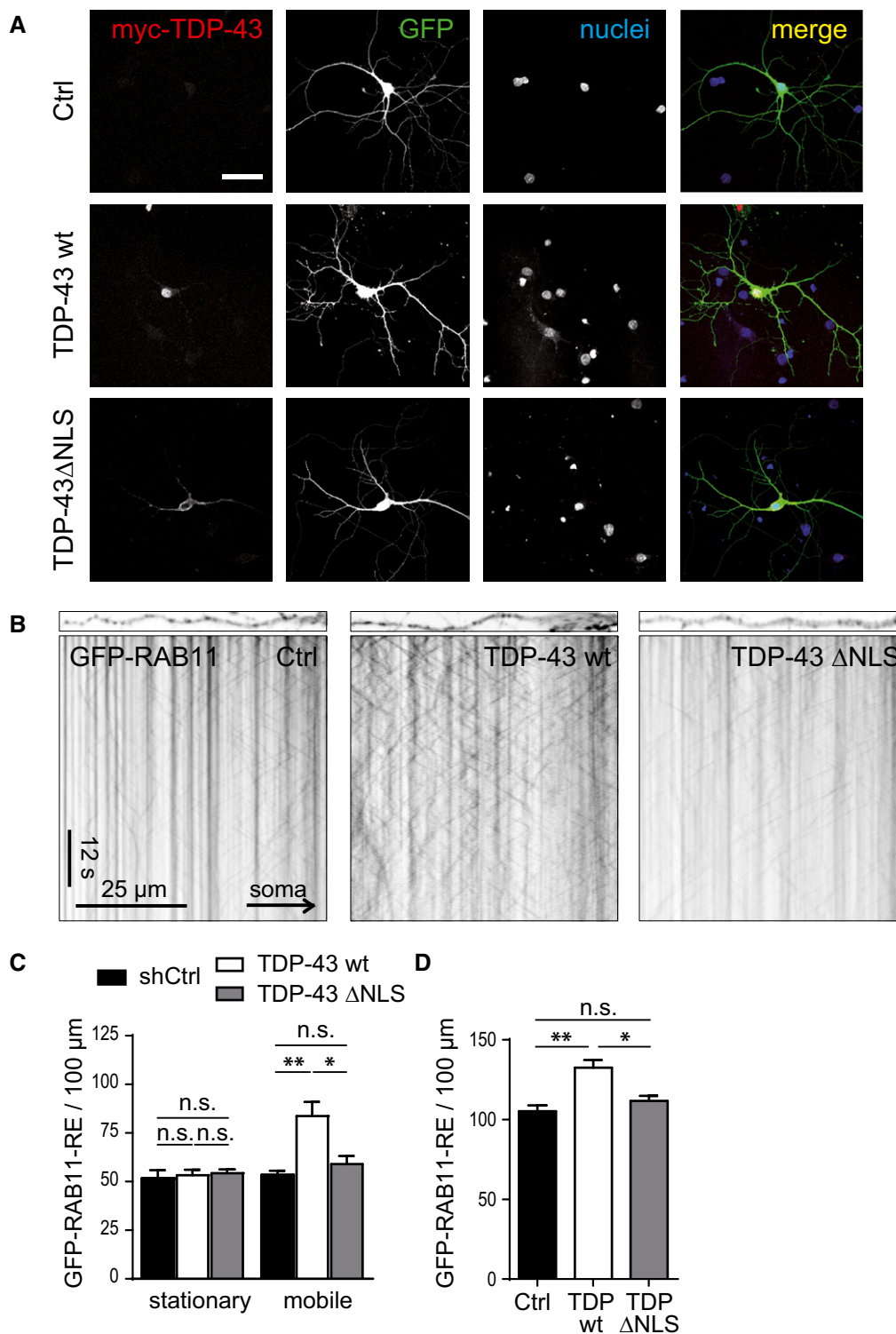
Figure 3. Expression of nuclear, but not cytoplasmic, TDP-43 enhances recycling endosome motility.

A   Primary hippocampal neurons (DIV6+4) were transfected with myc-tagged TDP-43 wild type or a mutant lacking the nuclear localization signal (ΔNLS) or an empty vector control. Immunostaining with the indicated antibodies and DAPI to label nuclei. Scale bar represents 50 μm.

B   Primary hippocampal neurons (DIV6+3) were transfected with either TDP-43 wild type, TDP-43ΔNLS, or an empty vector control together with GFP-RAB11 to visualize recycling endosomes and analyzed as in Fig 1.

C, D   Quantitative analysis of recycling endosome movement (C) and vesicle number (D). Mean ± s.e.m., *n* = 4, one-way ANOVA with Tukey's post-test: *$P < 0.05$, **$P < 0.01$.
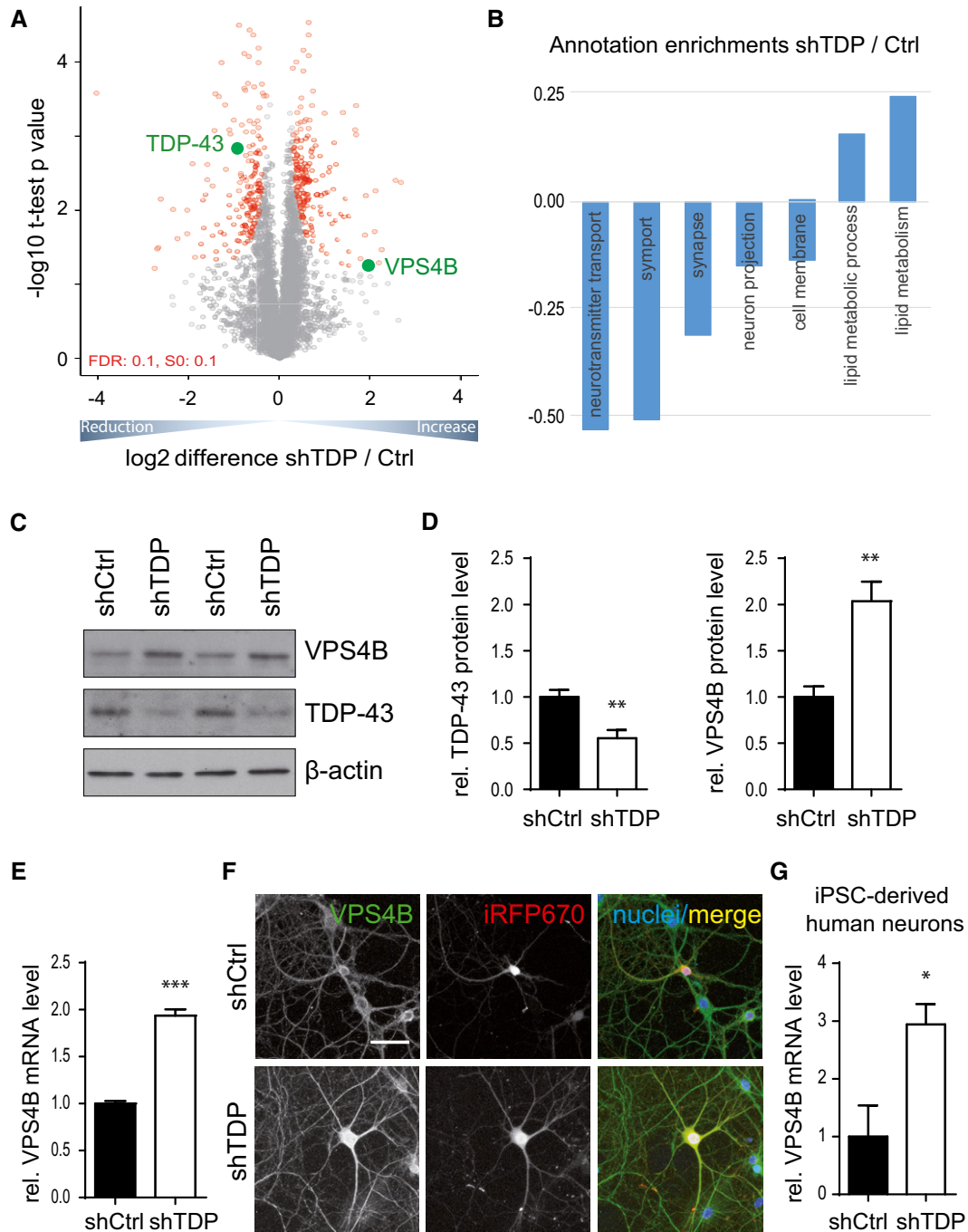
Figure 4. VPS4B is increased upon TDP-43 knockdown.

A   Primary cortical neurons were transduced with shTDP or control (DIV2+7) and subjected to quantitative proteomic analysis. Volcano plot shows up- and downregulated proteins from three biological replicates. Significant changes are colored. Compare with Table EV1.

B   Selected significantly enriched annotation between TDP-43 knockdown and control in proteomic data (complete data in Table EV1)

C–E   Primary hippocampal neurons (DIV6+4) were transduced with lentivirus expressing shRNA targeting TDP-43 or a control. Immunoblots with the indicated antibodies (C). Quantification of VPS4B and TDP-43 protein level using densitometry ($n = 4$). Expression was normalized to the housekeeping gene β-actin (D). VPS4B mRNA level were analyzed by quantitative RT-PCR. Expression was normalized to the housekeeping genes YWHAZ and PGK1 (E).

F   Primary hippocampal neurons (DIV6+3) were transfected with either shTDP or shCtrl and iRFP670. Immunostaining with the indicated antibodies. Scale bar represents 50 μm.

G   iPSC-derived human neurons were transduced 7 days after thawing for 3 days with shRNA targeting human TDP-43 (shTDP) or control (shCtrl). VPS4B levels were analyzed by quantitative RT-PCR. Expression was normalized to the housekeeping genes YWHAZ and PGK1 ($n = 3$).

Data information: Mean ± s.e.m., unpaired, two-tailed *t*-test with permutation-based (A) or Benjamini–Hochberg (B) correction: *$P < 0.05$, **$P < 0.01$, ***$P < 0.001$. Source data are available online for this figure.
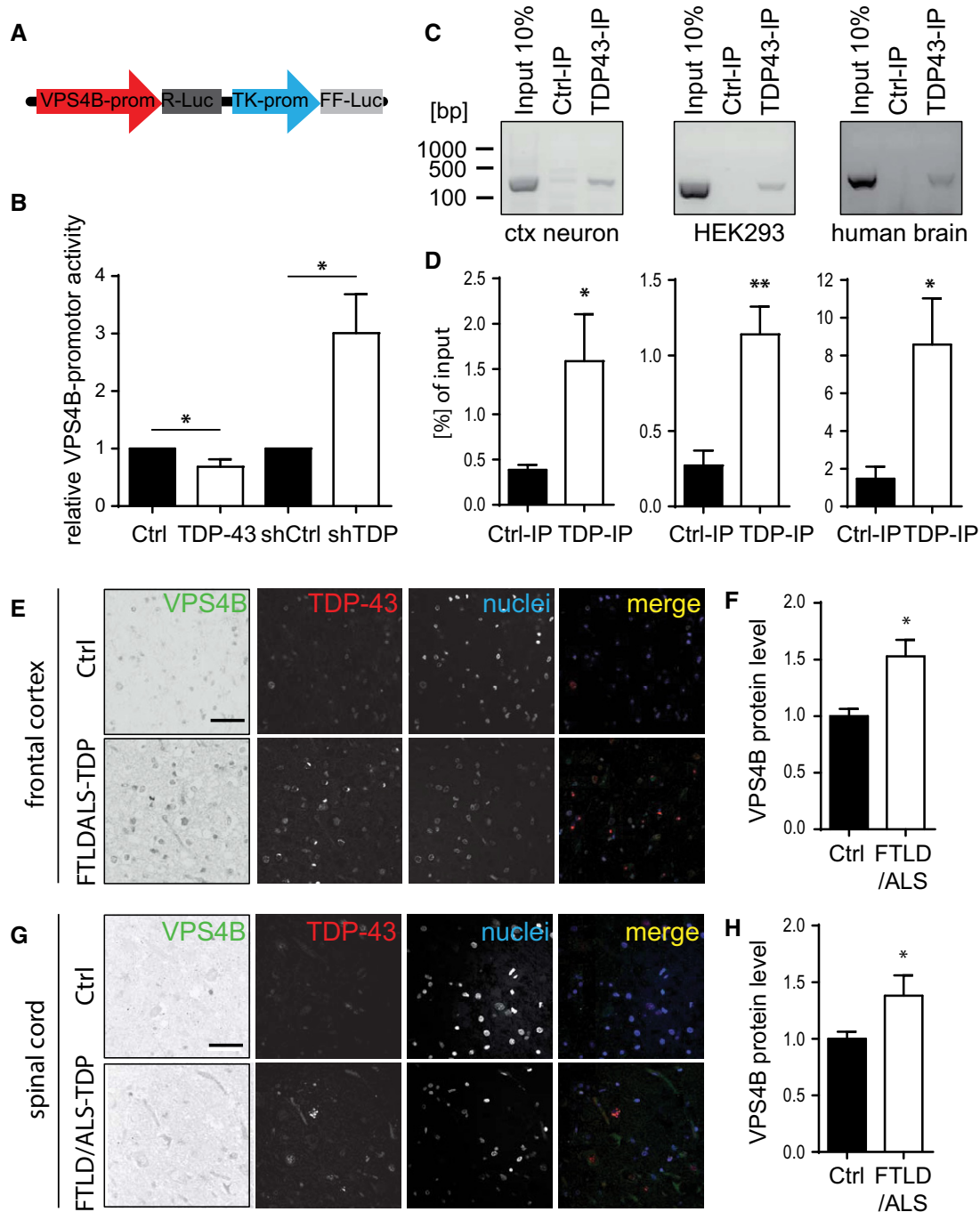
Figure 5. TDP-43 represses VPS4B expression by binding to the promoter region.

A, B   Luciferase assay to analyze transcriptional regulation of VPS4B by TDP-43. (A) Reporter construct expressing Renilla luciferase (R-Luc) driven by a VPS4B promoter fragment and firefly luciferase (FF) under the TK promoter. (B) HEK293 cells were transfected with shRNAs targeting human TDP-43, a control shRNA, TDP-43 wild type, or empty vector control together with the luciferase reporter containing the rat VPS4B promoter. VPS4B promoter-driven Renilla luciferase activity was normalized to TK promoter-driven firefly luciferase. Quantification from six independent experiments.

C, D   ChIP assay to analyze binding of TDP-43 to VPS4B promoter region in rat cortical neurons, HEK293 cells, and human brain tissue. PCR from input, negative control, and TDP-43 immunoprecipitates. Signal intensities from at least three independent experiments for each condition were quantified by densitometry and depicted as percentage of input.

E–H   Analysis of VPS4B in the tissues of seven patients with the neuropathological diagnosis of FTLD/ALS-TDP and five healthy controls. (E, G) Immunofluorescence with the indicated antibodies in the superior frontal gyrus or spinal cord. Scale bar represents 50 μm. (F, H) Quantification of cellular VPS4B levels. At least 50 cells per case were analyzed.

Data information: Mean ± s.e.m., unpaired, two-tailed *t*-test: *$P < 0.05$, **$P < 0.01$.
Source data are available online for this figure.

enrichment of VPS4B promoter DNA in TDP-43 immunoprecipitates (Fig 5D).

Next, we analyzed VPS4B in the frontal cortex and spinal cord of autopsy-confirmed FTLD/ALS-TDP cases. Immunostaining revealed an increased VPS4B expression in patients compared to age-matched controls in both regions (Fig 5E–H). In contrast, ALS-TDP cases lacking TDP-43 pathology in the frontal cortex showed VPS4B upregulation only in the spinal cord, but not in the frontal cortex (Fig EV4A–D). Moreover, we detected a similar upregulation of VPS4B in FTLD/ALS-TDP cases compared to controls by immunoblotting in the superior frontal gyrus (Fig EV4E and F). Together, these data strongly suggest that nuclear TDP-43 suppresses basal transcription of VPS4B, an important component of the ESCRT-III complex implicated in recycling endosome trafficking.

VPS4B mediates the recycling endosome impairment upon TDP-43 knockdown

To test whether VPS4B induction upon TDP-43 knockdown contributes to the reduction in recycling endosome motility in dendrites, we analyzed trafficking of GFP-RAB11 three days after transfection of a VPS4B expression vector (Fig 6A). Similar to the effects of TDP-43 knockdown, the number of moving recycling endosomes in VPS4B-transfected cells was significantly reduced compared to controls (Fig 6B and C).

To further corroborate our hypothesis that VPS4B induction mediates the effects of TDP-43 knockdown on RAB11-positive vesicle transport, we performed rescue experiments using VPS4B-specific shRNA (Fig EV4G and H). Importantly, additional knockdown of VPS4B in TDP-43-knockdown neurons restored the number and motility of recycling endosomes to control levels (Fig 6D–F). Next, we manipulated ALIX, a negative regulator of VPS4B that promotes ESCRT assembly, to strengthen the link to the ESCRT complex. Overexpression of ALIX enhanced RAB11-GFP motility in TDP-43-knockdown neurons nearly to control conditions and fully restored the vesicle number (Appendix Fig S3A–C).

Taken together, our data show that an enhanced expression of VPS4B is necessary and sufficient for the reduced recycling endosome number and motility upon TDP-43 knockdown, which is likely due to an enhanced ESCRT-III disassembly.

TDP-43 controls surface expression of ErbB4 and several other neuronal proteins

In neurons, recycling endosomes mediate constitutive and activity-dependent transport of many receptors to the plasma membrane. We speculated that impaired recycling endosome mobility upon TDP-43 loss of function would lead to a decreased cell surface expression of crucial receptors. We thus used proteomics to identify differentially expressed surface protein as targets of the TDP-43/VPS4B axis.

We therefore metabolically labeled all glycoproteins with a modified glycan and tagged their cell surface fraction with a non-membrane-permeable biotin using click chemistry (Kuhn *et al*, 2012). Labeled surface proteins were pulled down with streptavidin and identified and quantified using LC-MS/MS. Among the 43 proteins that were changed at high significance level ($P < 0.001$),

only two were upregulated, while the vast majority was downregulated, consistent with impaired recycling to the plasma membrane (Fig 7A and Table EV2).

We focused our analysis on ErbB4 and FGFR1, two of the most downregulated proteins on the cell surface, because they have been linked to motoneuron survival (Teng *et al*, 1999) or ALS. Pathogenic mutations in ErbB4 in patients with familial ALS were shown to block ErbB4 signaling in response to its ligand neuregulin 1 (NRG1; Takahashi *et al*, 2013). FGFR1 signaling has been linked to motor axon guidance (Shirasaki *et al*, 2006).

To provide further evidence for reduced surface expression (and activity) of the receptor tyrosine kinases ErbB4 and FGFR1, we analyzed autophosphorylation after 10-min stimulation with the ligands NRG1 and fibroblast growth factor-1 (FGF1) (Fig 7B–E). ErbB4 and FGFR1 phosphorylation was significantly reduced upon ligand treatment in TDP-43-knockdown neurons although total ErbB4 and FGFR1 protein levels were similar. To exclude transcriptional effects upon TDP-43 knockdown, we measured mRNA level of several of the most differentially expressed proteins (Fig 7F). While ErbB4, FGFR1, and most other tested mRNAs did not differ significantly between TDP-43 knockdown and control, c-Met and TMEM2 showed regulation in the same direction as the protein level arguing for a transcriptional effect in these cases.

To further corroborate the decreased surface expression of ErbB4 upon TDP-43 knockdown, we transfected neurons with ErbB4 tagged with a luminal HA-tag and a thrombin cleavage site (HA/T-ErbB4) together with the shRNA constructs and stained surface HA/T-ErbB4 using antibody feeding in live cells followed by staining of intracellular HA/T-ErbB4 in fixed cells. Consistent with the proteomic data, HA/T-ErbB4 surface levels were reduced in shTDP-transfected neurons compared to controls (Fig 7G and H). Next, we used a thrombin cleavage assay (Passafaro *et al*, 2001) to directly address trafficking of ErbB4. After removing the HA epitope of surface-expressed HA/T-ErbB4 in living cells using thrombin, we observed a delayed recovery of surface HA/T-ErbB4 from intracellular pools in TDP-43-knockdown neurons compared to controls (Fig 8A and B). Importantly, overexpression of VPS4B also led to a reduced surface expression of HA/T-ErbB4 (Fig EV5A and B), suggesting it is the main factor behind the effects of TDP-43 on surface localization of trophic receptors.

Thus, the cell surface expression of FGFR1 and the ALS-associated protein ErbB4 are reduced in TDP-43-knockdown neurons due to the impaired trafficking of recycling endosomes.

Impaired NRG1/ErbB4 signaling causes dendrite loss in TDP-43-knockdown neurons

Since NRG1/ErbB4 signaling promotes dendrite growth in neurons (Krivosheya *et al*, 2008; Cahill *et al*, 2012), we quantified the complexity of dendritic branching upon TDP-43 knockdown using Sholl analysis, as a functional readout of ErbB4 localization and activity. To that end, we transfected neurons (DIV6+4) with TDP-43 shRNA or control and GFP to visualize the whole cell and acquired images of individual cells. TDP-43 knockdown strongly reduced dendritic complexity (Fig 9A and B) similar to findings in flies (Lu *et al*, 2009). Overexpression of VPS4B or dominant-negative RAB11 mimicked this phenotype (Fig 9C and D and Appendix Fig S4A and
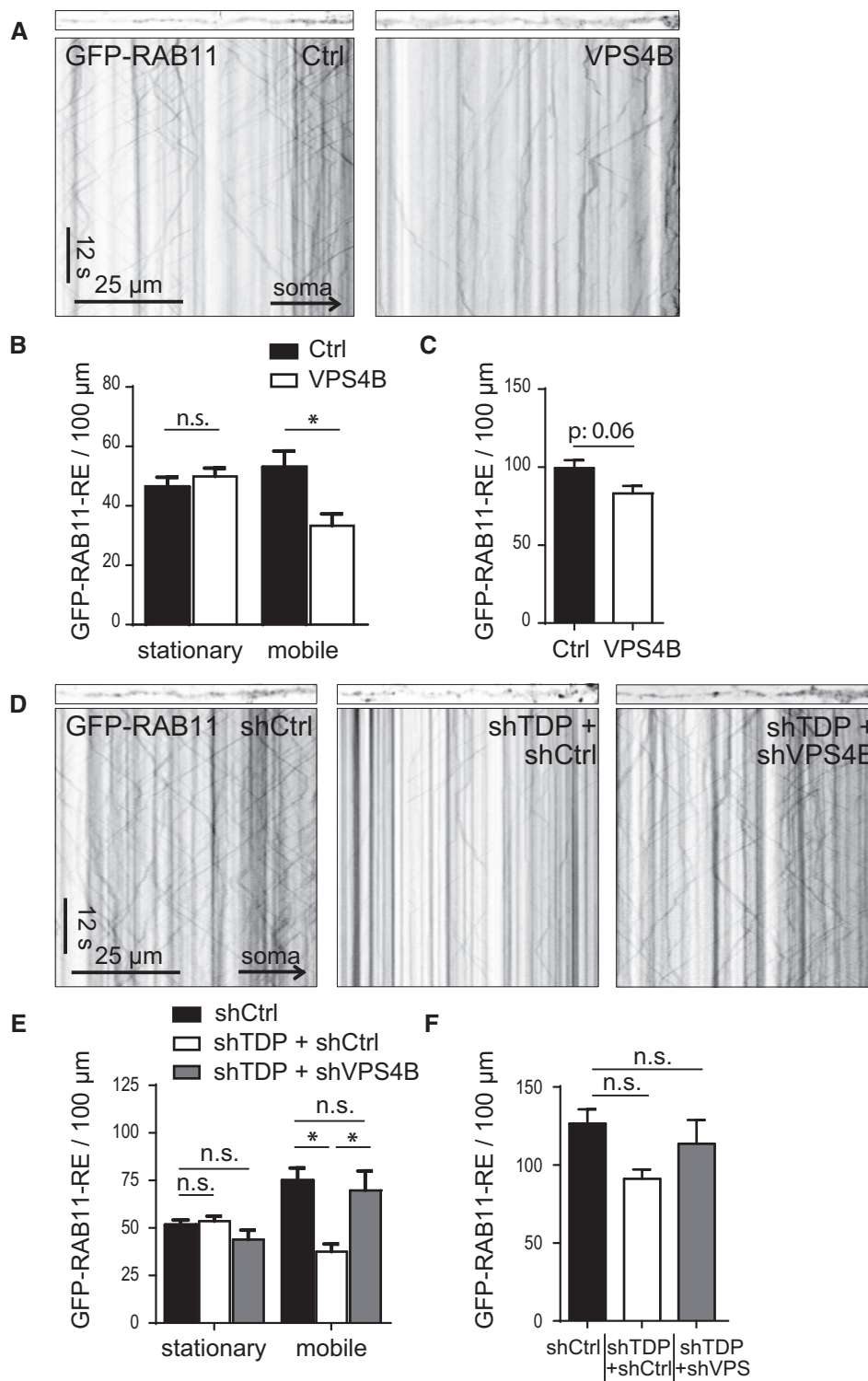
Figure 6. VPS4B upregulation is necessary and sufficient for impaired recycling endosome trafficking upon TDP-43 knockdown.

A   Primary hippocampal neurons (DIV6+3) were transfected with either VPS4B or an empty vector control together with GFP-RAB11 to visualize recycling endosomes. Neurons were imaged as in Fig 1 to analyze recycling endosome transport.

B, C   Quantitative analysis of vesicle motility (B) and the number (C) from kymographs in (A) ($n = 4$).

D   Primary hippocampal neurons (DIV6+3) were transfected with the indicated combinations of shRNA targeting TDP-43, VPS4B, and control together with GFP-RAB11 and imaged as in Fig 1.

E, F   Quantitative analysis of vesicle motility (E) and the number (F) from kymographs in (D) ($n = 3$).

Data information: Mean ± s.e.m., unpaired, two-tailed t-test (B, C) or one-way ANOVA (Tukey's post-test) (E, F): *$P < 0.05$.

The EMBO Journal
TDP-43 regulates trafficking of recycling endosomes
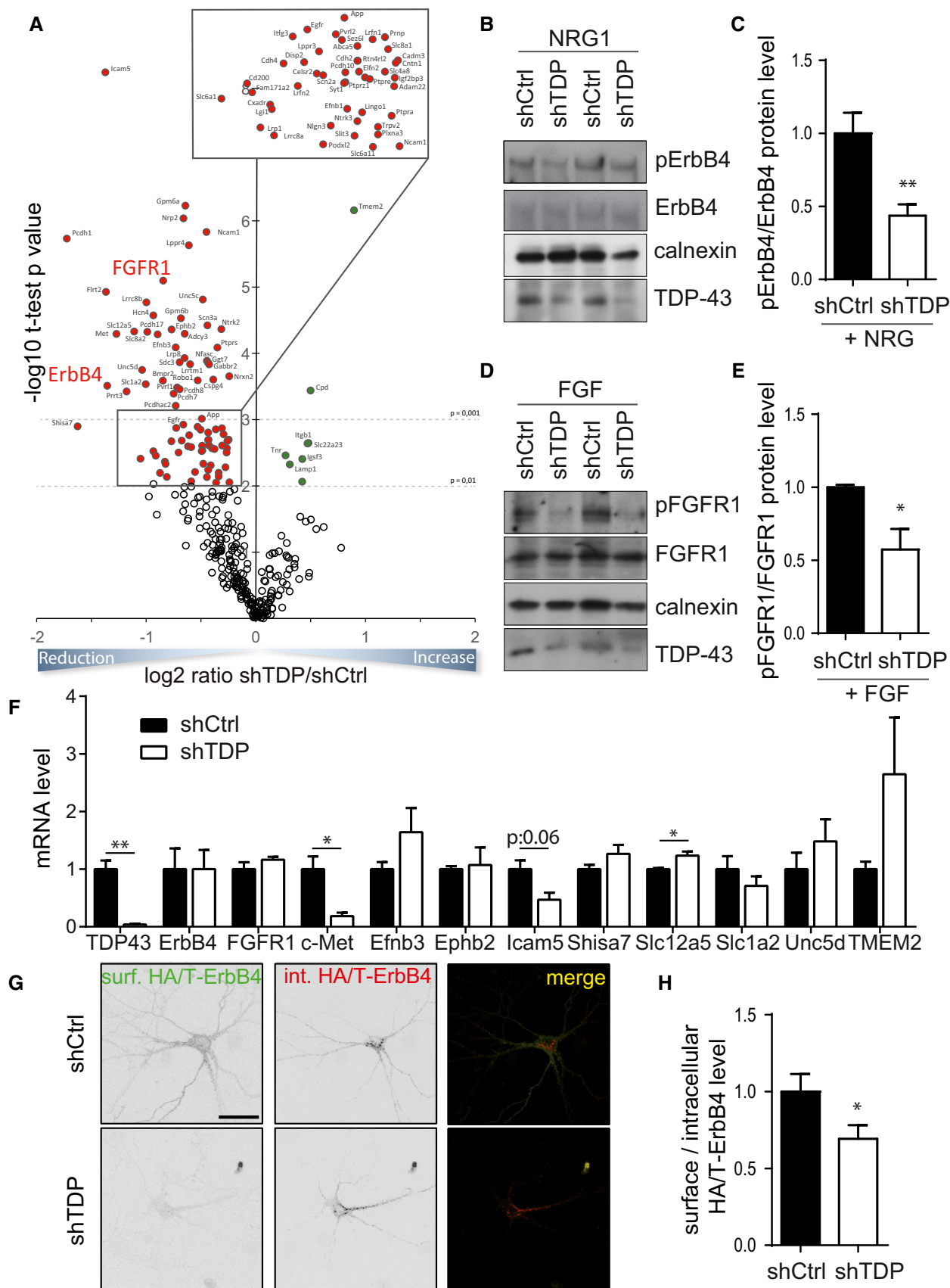Benjamin M Schwenk et al

Figure 7.

◄

Figure 7. TDP-43 knockdown reduces surface expression and the activity of ErbB4 and FGFR1.

A   Primary hippocampal neurons (DIV6+4) were transduced with shRNA targeting TDP-43 (shTDP) or control (shCtrl) and surface expression levels of glycoproteins were analyzed by metabolic labeling followed by surface biotinylation and subsequent streptavidin purification. Volcano plot depicts proteins that are significantly ($P < 0.01$, t-test, Benjamini–Hochberg, FDR: 0.05) decreased or increased on the cell surface in three independent experiments with two technical replicates. For full dataset, see Table EV2.

B–E   Primary cortical neurons (DIV6+5) were transduced with shCtrl or shTDP. Neurons were treated with the ErbB4 ligand NRG1 (10 nM) or FGFR1 ligand FGF1 (10 ng/ml) for 10 min right before cell lysis. Immunoblots with the indicated antibodies (B, D). Quantification of total and phospho-ERBB4 (Y1056) and total and phospho-FGFR1 (Y654) using densitometry of three to seven biological replicates (C, E).

F   Primary hippocampal neurons (DIV6+4) were transduced with shTDP or shCtrl. Gene expression was analyzed by quantitative RT–PCR normalized to the housekeeping genes YWHAZ and GAPDH ($n = 3$).

G   Hippocampal neurons were transfected with ErbB4 containing a luminal HA-tag (HA/T-ErbB4) and shCtrl or shTDP (DIV9+3). Surface HA/T-ErbB4 was stained in living cells and intracellular HA/T-ErbB4 was stained after fixation and permeabilization with HA antibodies. Scale bar represents 50 μm.

H   Quantification of HA/T-ErbB4 surface levels. At least 10 images per condition per experiment were analyzed in three independent experiments

Data information: Mean ± s.e.m., unpaired, two-tailed *t*-test: *$P < 0.05$, **$P < 0.01$.
Source data are available online for this figure.

B). Moreover, knockdown of TDP-43 in older neurons, when mature dendritic spines are already established (DIV14+5), led to a similar withering of the dendritic tree and significant spine loss (Appendix Fig S4C–F). The remaining dendritic spines were significantly thinner, indicative of reduced synaptic strength (Appendix Fig S4G and H).

While treating control neurons with the ErbB4 ligand NRG1 for two days enhanced the dendrite growth, NRG1 failed to promote dendrite growth in TDP-43-knockdown neurons (Fig 9E and F), suggesting that NRG1 signaling via ErbB4 is impaired. These effects were fully mimicked by VPS4B overexpression (Fig EV5C and D). In contrast, expression of ErbB4 in TDP-43-knockdown neurons led to the complete rescue of the dendritic complexity although ErbB4 expression in the control cells only slightly enhanced branching (Fig 9G and H). Similarly, ErbB4 expression was able to restore dendrite branching in VPS4B-transfected neurons (Fig EV5E and F). Thus, dendrite loss in TDP-43-knockdown neurons is at least partially due to the impaired recycling of ErbB4 to the plasma membrane caused by VPS4B upregulation.

Discussion

Loss of TDP-43 function is thought to be a major driver of neurodegeneration in FTLD and ALS patients with cytoplasmic TDP-43 aggregation, although the molecular mechanisms are poorly understood. Our data establish TDP-43 as an important regulator of recycling endosome dynamics by transcriptionally repressing the CHMP2B-interacting protein VPS4B. Impaired trafficking of recycling endosomes upon TDP-43 knockdown inhibits the cell surface expression of ErbB4 and hence prevents the stimulation of dendrite growth by its ligand NRG1. Thus, we directly link TDP-43 loss of function toxicity to two genes with rare ALS/FTLD-causing mutations, *CHMP2B* and *ErbB4*. This suggests a common pathway leading to neurodegeneration by blocking trophic signaling through the impaired dynamics of recycling endosomes.

Nuclear TDP-43 specifically controls dendritic trafficking of recycling endosomes

We show that TDP-43 loss of function impairs the trafficking of GFP-RAB11-positive recycling endosomes in the dendrites without

affecting the RAB4- and RAB5-positive endosome pools or mitochondria using live imaging in neurons. Impaired recycling of fluorescently labeled transferrin despite the normal initial internalization in TDP-43-knockdown neurons largely excludes confounding effects of ectopic GFP-RAB11 expression on endosome dynamics. Importantly, TDP-43 knockdown in iPSC-derived human neurons also impaired recycling endosome motility, further strengthening the relevance of this pathway for human pathophysiology. We discovered that altered endosomal dynamics upon TDP-43 knockdown is due to upregulation of VPS4B, an ESCRT-III disassembly factor. TDP-43 knockdown resulted in a significant dendrite loss that was phenocopied by the expression of VPS4B or dominant-negative RAB11, suggesting that endosome recycling is critical for dendrite development. We also observed a pronounced loss of dendritic spines in TDP-43-knockdown cells, which might be explained by the loss of synaptic receptors. Interestingly, acute chemical inactivation of RAB11 in neurons inhibits the surface delivery of AMPA receptors (Esteves da Silva *et al*, 2015).

Moreover, we noticed slightly increased motility of lysosomes, which might relate to the autophagosome–lysosome fusion problems observed in TDP-43-knockdown cell lines recently (Xia *et al*, 2015). Chronic dysfunction of the cellular degradation system is thought to promote TDP-43 aggregation (Filimonenko *et al*, 2007; Tashiro *et al*, 2012), but further lysosomal dysfunction due to nuclear clearance of TDP-43 might fuel a vicious cycle.

TDP-43 regulates the ESCRT factor VPS4B

To uncover the molecular mechanism of recycling endosome stalling, we analyzed the whole proteome of TDP-43-knockdown neurons using label-free quantitative proteomics. Among the differentially expressed proteins, we focused on VPS4B, because it had been linked to endosomal dynamics previously (Stuchell-Brereton *et al*, 2007; Du *et al*, 2013). VPS4B mRNA and protein levels are threefold upregulated in TDP-43-knockdown neurons from rats and humans. Enhanced VPS4B promoter activity upon TDP-43 knockdown suggests the transcriptional regulation of VPS4B by TDP-43. Chromatin immunoprecipitation shows that TDP-43 directly binds to a GT-rich region in the VPS4B promoter region in rat primary neurons and human brain, as shown before for TAR-DNA motif of HIV1 (Ou *et al*, 1995). Overexpression of VPS4B in neurons inhibits recycling endosome transport similar
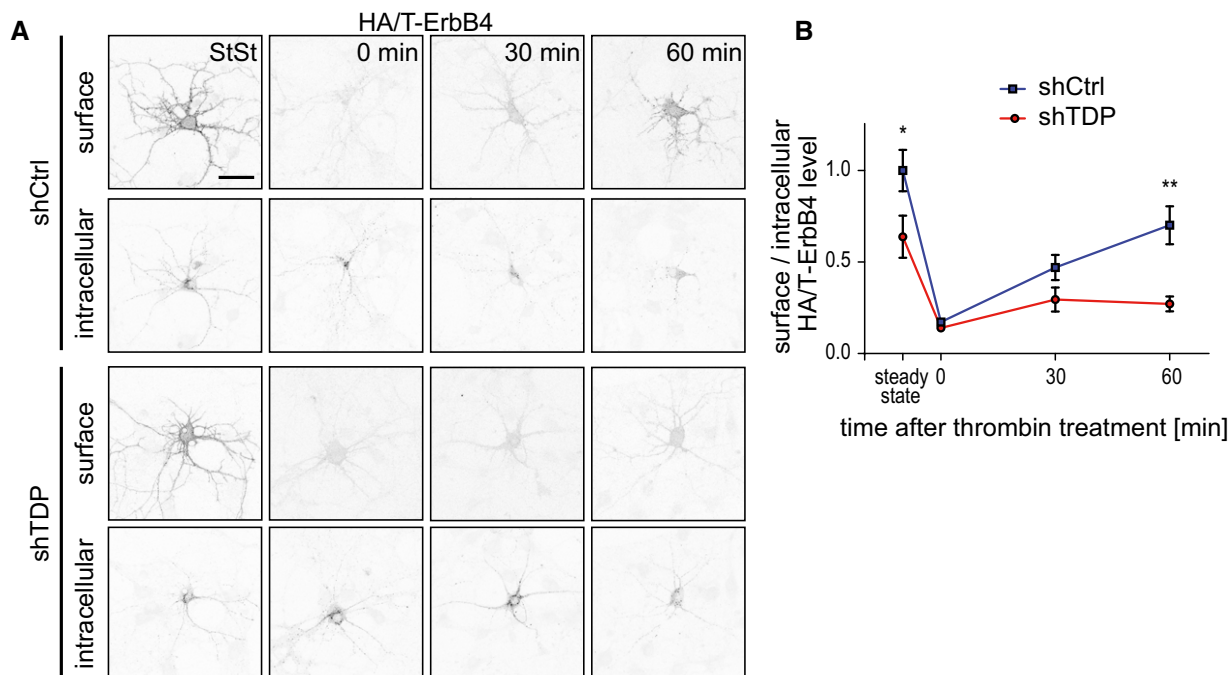
Figure 8. TDP-43 knockdown delays the surface delivery of ErbB4.

A, B   Primary hippocampal neurons (DIV6+3) were transfected with shCtrl or shTDP and ErbB4 containing an N-terminal HA epitope tag and followed by thrombin cleavage site (HA/T-ErbB4). Surface HA/T-ErbB4 was stained in living cells and intracellular HA/T-ErbB4 was stained after fixation and permeabilization with two different HA antibodies. After removing the HA signal of surface ErbB4 (0 min) using thrombin cleavage (5 min, 1 U/ml), membrane insertion of HA/T-ErbB4 was measured at the indicated time points. The steady state (StSt) before thrombin cleavage is also depicted. At least 10 images per condition per experiment were analyzed in three independent experiments. Scale bar represents 50 μm. Mean ± s.e.m., unpaired, two-tailed t-test: *$P < 0.05$, **$P < 0.01$.

to TDP-43 knockdown. Importantly, preventing VPS4B upregulation using shRNA completely rescues recycling endosome motility in TDP-43-knockdown neurons, strongly suggesting that VPS4B upregulation is the major cause of the trafficking deficits upon TDP-43 knockdown.

VPS4 controls normal endosomal trafficking and sorting and is required for disassembly of the ESCRT-III complex (Yoshimori *et al*, 2000; Jouvenet, 2012). Promoting ESCRT assembly by ALIX overexpression also largely restored the trafficking deficits in TDP-43-knockdown cells (Adell & Teis, 2011). VPS4B directly interacts with the ALS-associated CHMP2B, another crucial part of the ESCRT-III complex, and this interaction is blocked by ALS/FTLD-causing mutations in CHMP2B (Skibinski *et al*, 2005; Stuchell-Brereton *et al*, 2007; Han *et al*, 2012). Several other VPS family members have been genetically linked to neurodegenerative disorders, for example, VPS35 to Parkinson's disease and the VPS10 proteins SORL1 and SORCS1 to Alzheimer's disease (Lane *et al*, 2012). Thus, linking TDP-43 loss of function to VPS4B, thus the ESCRT complex, and impaired recycling endosome motility further highlights the role of vesicle trafficking in neurodegeneration.

TDP-43 loss of function impairs cell surface expression of key receptors for growth and guidance factors

The balance of endocytosis and recycling regulates the homeostasis of adhesion molecules and receptors for neurotransmitters, growth factors, and guidance cues (Goh & Sorkin, 2013). To identify the proteins most affected by impaired recycling endosome dynamics in neurons, we analyzed the changes in the surface proteome upon TDP-43 knockdown using proteomics (Kuhn *et al*, 2012). Reduced surface expression is likely due to the impaired recycling, because TDP-43 knockdown has no apparent effect on transferrin endocytosis or on trafficking of RAB5-positive early endosomes. We found a highly significant reduction of 43 proteins on the surface, many of them known cargoes of recycling endosomes, while only two surface proteins were significantly upregulated. Among the proteins with reduced surface expression upon TDP-43 knockdown, only two of ten tested mRNAs were significantly downregulated, suggesting that the trafficking effects are dominant.

More than half of the proteins with reduced surface expression are involved in dendrite growth (e.g., ErbB4, FGFR1, EphB2) or axonal guidance (e.g., Robo1, Unc5c/d, EphB2, TrkB). In flies, TDP-43 knockout impairs the dendrite growth by a cell autonomous mechanism (Lu *et al*, 2009). We found that TDP-43 knockdown in rat primary neurons also leads to the loss of dendrites and dendritic spines, thus potentially compromising synaptic transmission. We focused on the receptor tyrosine kinase ErbB4, one of the most downregulated proteins on the cell surface, because it had previously been linked to ALS through rare pathogenic mutations in its kinase domain that inhibit response to its ligand NRG1 (Takahashi *et al*, 2013). Although ErbB4 is predominantly expressed in interneurons and motor neurons, the lower level of ErbB4
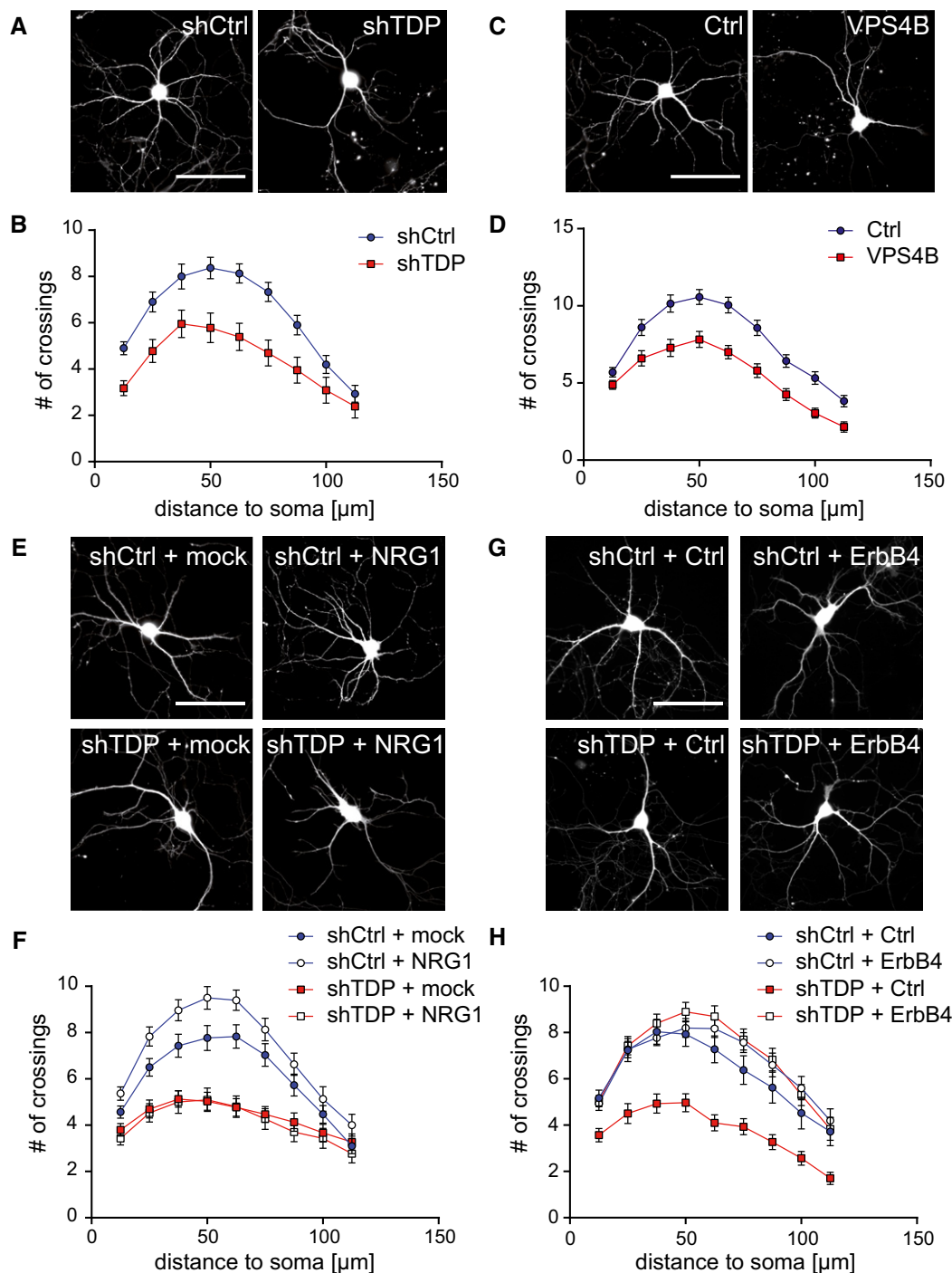
Figure 9. TDP-43 knockdown blunts dendritic complexity and response to NRG1.

Primary hippocampal neurons (DIV6+4) were cotransfected with shTDP, VPS4B, or appropriate controls and GFP to visualize neuron morphology. Dendritic morphology from at least 23 neurons per condition per experiment was quantified by Sholl analysis and statistically evaluated using two-way ANOVA with Bonferroni's (B, D) or Tukey's (F, H) post-test. Scale bar represents 100 μm. Mean ± s.e.m..

A, B   TDP-43 knockdown (DIV6+5) significantly reduces dendrite branching compared to control: at 25, 37.5, and 87.5 μm radius $P < 0.05$, at 50 μm $P < 0.01$, and from 62.5 to 75 μm $P < 0.001$.

C, D   VPS4B transfection (DIV6+4) significantly reduces dendrite complexity: at 25 μm radius $P < 0.05$, from 37.5 to 75 μm $P < 0.001$, and from 87.5 to 100 μm $P < 0.01$.

E, F   Two days after shRNA transfection, the neurons were treated with 1 nM NRG1-beta 1 (NRG1) or vehicle and analyzed at DIV6+5. shCtrl vs. shTDP: at 25 and 87.5 μm radius $P < 0.05$, from 37.5 to 75 μm $P < 0.001$. shCtrl vs. shCtrl + NRG1: from 37.5 to 62.5 μm $P < 0.05$. shTDP vs. shTDP+NRG1: no significant difference.

G, H   Transfection of the indicated combinations of shCtrl, shTDP, ErbB4, or vector control (DIV6+5). shCtrl + Ctrl vs. shTDP + Ctrl: from 25 to 75 μm radius $P < 0.001$, at 87 and 112.5 μm $P < 0.01$, and at 100 μm $P < 0.05$. shTDP + Ctrl vs. shTDP + ErbB4: from 25 to 100 μm radius $P < 0.001$, at 112.5 μm $P < 0.01$. shCtrl + Ctrl vs. shTDP + ErbB4: no significant differences.

expression in excitatory neurons is still crucial to regulate dendritic spine morphology and synaptic plasticity (Li *et al*, 2007; Cooper & Koleske, 2014). We observed an enhanced dendritic branching upon NRG1 treatment in excitatory control neurons, similar to previous findings (Gerecke *et al*, 2004; Krivosheya *et al*, 2008; Allison *et al*, 2011). In contrast, the stunted dendrite growth in TDP-43-knockdown cells could not be stimulated by NRG1 treatment, indicating that an impaired trafficking of recycling endosomes blocks the NRG1/ErbB4 signaling axis. Importantly, increasing ErbB4 levels in TDP-43-knockdown neurons restored dendritic arborization to control conditions, suggesting that reduced ErbB4 surface expression is a major cause for the dendrite withering in our system. We could reproduce all ErbB4-related findings also in VPS4B-overexpressing neurons, strongly suggesting that VPS4B upregulation and its effect on endosome trafficking directly inhibit receptor recycling upon TDP-43 knockdown.

TDP-43 knockdown reduced surface expression of many other receptors for growth and guidance cues and thus presumably has more widespread effects on trophic signaling. Depending on cell type and age, other plasma membrane proteins undergoing recycling might be affected. For example, the reduced levels of CADM3 found in the CSF of ALS patients (Collins *et al*, 2015) could be explained by the reduced cell surface expression (Fig 7A) and subsequent shedding upon the loss of nuclear TDP-43. Additionally, we found reduced mRNA expression and surface expression of the hepatocyte growth factor (HGF) receptor c-Met. Interestingly, muscle-derived HGF promotes the axon outgrowth and survival of motoneurons during development via c-Met (Ebens *et al*, 1996) and HGF/c-Met expression declines with disease progression in ALS patients (Kato *et al*, 2003). Many of these signaling pathways have been most extensively studied during development, but remain essential in adulthood and might be even more critical upon injury or neuronal damage. For example, FGF signaling is crucial for motoneuron protection and survival after spinal cord injury (Teng *et al*, 1999). Thus, the impaired activity of ErbB4, FGFR1, c-Met, and other receptor tyrosine kinases may deprive neurons with TDP-43 mislocalization and aggregation from crucial trophic support leading to progressive neuron loss. Interestingly, the removal of established TDP-43 aggregates and the subsequent restoration of nuclear TDP-43 expression lead to functional reinnervation in an inducible mouse model, further supporting a role of TDP-43 in trophic signaling (Walker *et al*, 2015).

Clinical implications

Three lines of evidence support that an impaired endosomal recycling occurs in ALS and FTLD patients. First, we observed the reduced recycling endosome motility and VPS4B upregulation upon TDP-43 knockdown in human iPSC-derived neurons. Second, region-specific elevation of VPS4B in sections of ALS-TDP and FTLD/ALS-TDP patients suggests that TDP-43 loss of function in patients with TDP-43 aggregation invokes a similar mechanism as in cultured neurons. Third, ALS patients have reduced transferrin levels in serum and CSF (Brettschneider *et al*, 2008; Nadjar *et al*, 2012), a result we confirmed in our cohort of sporadic ALS patient for the CSF-specific β2-transferrin. This finding can now be explained by the impaired transferrin transport and recycling caused

by TDP-43 loss of function. Moreover, our findings could also be relevant for Alzheimer's disease, as TDP-43 aggregation and nuclear clearance are found in up to 50% of cases (Davidson *et al*, 2011).

Our work establishes a connection between TDP-43, impaired vesicle trafficking, and dendrite growth by controlling cell surface expression of receptors crucial for neurite outgrowth and neuronal survival. Impaired recycling of trophic receptors to the cell surface due to nuclear clearance of TDP-43 and VPS4B upregulation in patients may compromise neuronal repair and survival in ALS and FTLD.

Materials and Methods

DNA constructs

Myc-tagged human TDP-43 wild type and the ΔNLS (97AAA) mutant cDNA were expressed from pcDNA6 vector driven by CMV promoter. Myc-tagged rat VPS4B, human HA/T-ErbB4 (HA-tag followed by a thrombin cleavage site (LVPRGS) were inserted directly after the signal sequence, cloned from Addgene plasmid #29527, Yardena Samuels (Prickett *et al*, 2009)), and human ALIX (subcloned from Addgene plasmid #21504, James Hurley (Lee *et al*, 2008)) cDNA was expressed from a lentivirus plasmid driven by ubiquitin promoter (Orozco *et al*, 2012). shRNAs were cloned into pSUPER (target sequences: rat TDP-43 #1 gtagatgtcttcattcccaaa, rat TDP-43 #2 gctgatgggctgcgaacat, human TDP-43: gaaacacaagtgaaag taa, rat VPS4B: ggtgcagatcagcgtgaca and luciferase control cgtacgcg gaatacttcga). For lentiviral knockdown, the H1 promoter shRNA expression cassette was subcloned into a lentiviral vector coexpressing mCherry from human ubiquitin C promoter (Orozco *et al*, 2012). Human RAB4 (Addgene #54943, M. Davidson unpublished), RAB5 (Lang *et al*, 2012), RAB7 and RAB11a wild type and S25N (Addgene #12605, 12674, 12678, Richard Pagano (Choudhury *et al*, 2002)) were expressed from pEGFP-C1 vector. Mito-GFP contains the mitochondrial targeting sequence of COX8. For the luciferase reporter construct, genomic sequence 1 kb upstream of the predicted TSS (http://www.cbs.dtu.dk/services/Promoter/) until the start codon of rat *VPS4B* was cloned in upstream of Renilla luciferase in the psiCheck2 vector (primers gatggatccctcccatac actacaaggggaagctc and gatgctagctggtggagatccaaagggtccccta). All constructs were verified by sequencing.

Lentivirus was produced by cotransfecting psPAX2, pVSV-G, and the respective overexpression or knockdown constructs in HEK293FT as described before (Schwenk *et al*, 2014). After harvesting the supernatant, virus particles were concentrated by ultracentrifugation and resuspended in PBS.

Antibodies and reagents

Antibodies against TDP-43 (Sigma-Aldrich Cat# SAB4200006, Cosmo Bio Co Cat# CAC-TIP-TD-P09), GFP (UC Davis/NIH NeuroMab Facility Cat# 73-132), β-actin (Sigma-Aldrich Cat# A5316), calnexin (Enzo Life Sciences Cat# ADI-SPA-860-F), VPS4B (Sigma-Aldrich Cat# PA5-30316 for IHC and Proteintech Group Cat# 17673-1-AP for immunoblotting and immunofluorescence), ErbB4 (Santa Cruz Biotechnology Cat# sc-283), phosphor-ErbB4-Y1056 (Santa Cruz

Biotechnology Cat# sc-33040), FGFR1 (Novus Cat# NB600-1287), phosphor-FGFR1-Y654 (Abcam Cat# ab59194), myc-tag (Santa Cruz Biotechnology Cat# sc-40), HA-tag (Sigma-Aldrich Cat# H9658 and Roche Cat# 3F10), anti-mouse and rabbit HRP-coupled secondary antibodies and anti-mouse and rabbit Alexa-coupled secondary antibodies (Life Technologies) are commercially available. TO-PRO 3 and transferrin-Alexa 555 were purchased from Life Technologies, and DAPI and EZ-Link sulfo-NHS-LC biotin from Sigma-Aldrich. β2-Transferrin protein levels from undiluted CSF samples derived from sporadic ALS patients and controls were quantified using a commercially available ELISA kit (www.mybiosource.com, MBS923983) following the manufacturer's instructions. Recombinant NRG1 and FGF1 were purchased from R&D Systems.

Neuron cell culture and imaging

Hippocampal neurons were prepared from embryonic day 18 CD rats (Charles River), cultivated in Neurobasal media (with 2% B27, 0.25% glutamine, 0.125% glutamate), and transduced with lentivirus or transfected with Lipofectamine 2000 as described before (Schwenk *et al*, 2014). Immunoblotting and immunostaining were performed as described previously (Schwenk *et al*, 2014). Images were taken on Zeiss LSM 510 or 710 confocal laser scanning microscopes using 40× (NA = 1.3) oil immersion objectives with 1 Airy unit pinhole. Dendritic arborization was quantified manually by Sholl analysis as described previously (Schwenk *et al*, 2014). In each experiment, at least 30 neurons per condition were imaged and quantified. Figures show the representative data from one of at least three independent replicates with similar results. All image acquisition and quantification for morphological analyses were done blind to the experimental conditions.

iPSC-derived human neurons were generated as described before (Koch *et al*, 2009) and frozen in liquid nitrogen for long-term storage. After thawing, neurons were plated on PDL-coated glass-bottom dishes in HN media (DMEM/F12 and Neurobasal 1:1, 0.5% N2, 1% B27, 0.1 % glucose, 2 μg/ml insulin, 10 ng/ml GDNF, 10 ng/ml BDNF, 10 μM Y-27632). Every two days half of the media were exchanged. Neurons were transduced with lentivirus seven days after thawing and imaged three days later.

Astrocyte feeder cells were prepared from embryonic day 18 CD rats (Charles River) as described previously (Kaech & Banker, 2006), plated onto glass coverslips, and maintained in MEM supplemented with 0.6% glucose and 5% FBS till they reached 50–60% confluency.

Live cell imaging

For vesicular motility analysis, images for time-lapse movies were taken on a Zeiss Cell observer SD spinning-disk microscope with an air-cooled Evolve 512 EMCCD camera at 5 Hz for 60 s (RAB11), 2 Hz for 150 s (RAB4, RAB5, mitochondria), or 1 Hz for 300 s (RAB7) with an 63× oil immersion objective (NA = 1.4). During image acquisition, neurons were kept in a climate chamber (37°C, 5% CO_2). Unless noted otherwise, kymographs of vesicular movement from at least four dendrite segments per cell and at least six neurons per condition and experiment were generated and manually analyzed using ImageJ software (Multiple Kymograph plugin by J. Rietdorf and A. Seitz).

Transferrin recycling assay

The protocol for transferrin recycling assay was adapted (Moreau *et al*, 2012). Neurons were transduced with the lentiviruses coexpressing shRNA and RFP. On day five, cells were starved in culture media without B27 (30 min at 37°C and 5% CO_2) prior to incubation with 50 μg/ml transferrin-Alexa-488 in complete culture media for 20 min at 4°C. Subsequently, neurons were put back at 37°C and 5% CO_2 for 20 min to allow transferrin internalization (pulse). Afterward, the cells were washed three times, put back in complete culture media (containing unlabeled transferrin as part of B27) for 0, 20, or 60 min (chase), and fixed (4% PFA, 4% sucrose) after another wash with PBS. Transferrin-Alexa-488 was quantified from confocal images by relating transferrin fluorescence signal to the cell area, visualized by RFP expression (not shown in Fig 2), and normalized to control transduced cells.

VPS4B promoter assay

A modified psiCHECK2-expressing Renilla luciferase from a 1-kb VPS4B promoter fragment and firefly luciferase from the TK promoter was cotransfected with control or TDP-43 constructs at a 40:60 ratio into HEK283FT cells using Lipofectamine 2000 (Life Technologies). On day 3, luciferase activity was quantified using Dual-Glo Luciferase Assay (Promega). Relative promoter activity was determined by normalizing the ratio of Renilla luciferase and firefly luciferase to the control vector and the effect on the original psiCHECK2 vector. All experiments were performed in 96-well plates with six replicates for each condition.

Chromatin immunoprecipitation (ChIP)

ChIP experiments in cortical neurons, HEK293 cells, and brain tissue were performed using the MAGnify Chromatin Immunoprecipitation System (Thermo Fisher Scientific) according to the manufacturer's instructions. Briefly, chromatin from 300,000 cells or 20 mg tissue per ChIP reaction was crosslinked by 1 % formaldehyde and sheared with a Branson WD200 sonifier (30% amplitude, 60% duty cycle, 4× 30-s impulse, 60-s recovery) to an approximate size of 300–500 bp. Following cell lysis, protein was immunoprecipitated using either rabbit polyclonal TDP-43 (Cosmo Bio, CAC-TIP-TD-P09) or rabbit control antibody. After five washing steps, the cross-link was reversed in immunoprecipitates and input samples followed by proteinase K digestion. Afterward, DNA was isolated and PCRs from input, control- and TDP-43-IP were performed amplifying ~200-bp amplicons in the promoter region of VPS4B. We detected binding with the following amplicons in rats (gcagagggaaacagaaatta, ctagctctattcacacacac) and humans (gctcgttc ccgcttgttc, tggtggctgcaaaccatag).

Surface staining and thrombin cleavage assay

The protocol for receptor surface quantification and thrombin cleavage assay was adapted from Passafaro *et al* (2001). In brief, hippocampal neurons (DIV7+4) were transfected with HA/T-ErbB4 and shTDP or shCtrl and incubated for 4 days. Cells were live-labeled with rat anti-HA antibody for 1 h at 4°C to visualize surface HA proteins, washed with cold Neurobasal media, and

fixed for 8 min in 4% PFA. Afterward, fixed neurons were incubated with mouse anti-HA to label intracellular receptors. The neurons were washed in 20 mM phosphate buffer containing 0.5 M NaCl (pH 7.4), incubated in Alexa-labeled secondary antibodies, and mounted. For the quantification of receptor recycling to the plasma membrane, HA/T-ErbB4-transfected hippocampal neurons were treated for 5 min with thrombin (Sigma-Aldrich; 1 U/ml), followed by three washing steps with warm Neurobasal. Subsequently, the cells were returned to 37°C to allow for membrane insertion of new receptors. Neurons were labeled as described above either without thrombin treatment, or 0, 30, or 60 min after thrombin treatment. Images were taken with a Zeiss LSM 710 confocal microscope.

Quantification of immunofluorescence images

Images were acquired on a Zeiss LSM 710 laser scanning confocal microscope using the same settings during the whole experiment. Fluorescence levels were quantified with ImageJ by using the background corrected total cell fluorescence. The total corrected cellular fluorescence (TCCF) = integrated density – (area of selected cell × mean fluorescence of background readings), was calculated (McCloy *et al*, 2014). All image acquisition and quantification were performed blinded to the experimental conditions.

RNA preparation and quantitative PCR

RNA was isolated using RNeasy Mini Kit with the optional DNase digest step (Qiagen) following the manufacturer's instructions. cDNA was generated using the TaqMan MicroRNA Reverse Transcription Kit (Applied Biosystems) with random hexamer primers following the manufacturer's instructions. RT–qPCR was performed on CFX384-Real-Time system using SsoFast EvaGreen (Bio-Rad) with a two-step protocol using the following primers: rat VPS4B (primers ccaccatggcgtccacgaacac and tggccctgatgctttgcttggc), rat TDP-43 (agtgttgggtctcccctggaaa, acagtcacaccatcgcccatct), rat YWAHZ (tgagcagaagacggaaggtgctg, tctgatggggtgtgtcggctgc), and rat GAPDH (ccgcatcttcttgtgcagtgcc, agactccacgacatactcagcacc). Amplification of a single product was confirmed by melting curve analysis. Relative mRNA abundance was quantified by the ΔΔCT method.

Human samples

Human CSF samples were provided by the MND-NET and the German FTLD consortium. All patient tissues were provided by the Neurobiobank Munich, Ludwig Maximilians University (LMU) of Munich. All samples were collected and distributed according to the guidelines of the local ethical committee.

Immunofluorescence of paraffin sections

Immunofluorescence was performed as previously described (Mackenzie *et al*, 2013). In short, paraffin sections were dewaxed in xylene and ethanol followed by microwaving in citrate buffer (pH 6). The VPS4B and TDP-43 antibodies were incubated overnight at 4°C, and the fluorescence-labeled secondary antibody 1 h at room temperature. Nuclei were stained with DAPI for 15 min.

Statistical analysis

Statistical analysis was performed using GraphPad Prism software. If sample size allowed, data were tested for normal distribution with D'Agostino–Pearson omnibus normality test. If data points were not normally distributed, a nonparametric test was used, when applicable. To compare one variable in two independent groups, the unpaired, two-sided *t*-test or Mann–Whitney *U*-test were used; in cases with three or more independent groups, one-way ANOVA or Kruskal–Wallis test were used. To compare groups using two variables, two-way ANOVA was applied. If necessary, tests were corrected for multiple comparisons using the Bonferroni or Tukey method owing to the applied test and the number of groups. A *P*-value < 0.05 was considered significant. Statistical analysis of proteomic data is described in detail below.

Whole proteome analysis by LC-MS/MS

Cells were lysed in SDS-containing buffer and subjected to tryptic digestion as described previously (Hornburg *et al*, 2014). We separated peptides on a HPLC (EASY-nLC 1000, Thermo Fisher Scientific, Odense, Denmark) using 50-cm columns (75-μm inner diameter) in-house packed with 1.9-μm C18 beads (Dr. Maisch GmbH, Ammerbuch-Entringen, Germany). Peptides were loaded in 0.5% formic acid (buffer A) and eluted within a 245-min gradient from 5% buffer B (80% acetonitrile, 0.5% formic acid) to 60% B at 250 nl/min. The column was heated to 50°C to reduce backpressure. Our setup employed a hybrid quadrupole Orbitrap mass spectrometer (Michalski *et al*, 2011) (Orbitrap Q Exactive, Thermo Fisher Scientific) directly coupled to the HPLC via nanoelectrospray source. The survey scan (MS1, 300 to 1,650 m/z) was performed at a resolution of 70,000 at m/z 200 and an ion target value of 3E6. Up to the top 10 most intense features with a charge state higher than one not picked previously (dynamic exclusion window 30 s) were subjected to HCD fragmentation (AGC target 1e5, isolation window 2.2 m/z) at a normalized collision energy of 25. Data were acquired using Xcalibur software (Thermo Scientific).

Whole proteome raw data analysis and statistical analysis

We processed the raw data with MaxQuant (Cox & Mann, 2008) (v. 1.4.1.6) and used the integrated search engine Andromeda (Cox *et al*, 2011) to search MS/MS spectra against the rat UniProtKB Fasta database (34,562 forward entries; version from July 2015). The enzyme specificity was set to trypsin while allowing up to two miscleavages and cleavage N-terminal to proline. We set the minimum length of peptides to be considered for identification to seven amino acids assuming carbamidomethylation of cysteine as fixed and methionine oxidation (M) as well as acetylation of N-termini as variable modifications. A false discovery rate (FDR) cutoff of 1% was applied on both the peptide and protein level.

We performed nonlinear retention time alignment of all measured samples in MaxQuant, which allows us to transfer peptide identifications in the absence of sequencing (MS1 only), within a narrow retention time window of 1 min ("match between runs"). We employed a library of 20 cortical rat neuron

proteomes as a library for matching. Protein intensities were normalized with MaxQuant (MaxLFQ; Cox *et al*, 2014). We stringently filtered our data requiring at least two peptide ratios for protein quantification. In addition, common contaminants ($n = 247$, included in MaxQuant software packages) as well as proteins only identified with side modifications were strictly excluded from the analysis. Furthermore, we removed any protein group with less than two-third valid values for either control or knockdown from the analysis. Remaining missing values were imputed with a normal distribution (based on whole data distribution, width = 0.3, downshift = 1.8).

For statistical analysis, we employed Perseus, which is part of the MaxQuant environment. To emphasize the strength of biological differences, we employed a S0 correction of 0.1 in the statistical analysis (Student's *t*-test) (Tusher *et al*, 2001). The biological difference between TDP-43 knockdown and control was mild and we had to choose a slightly less stringent multiple testing correction (permutation-based FDR of 0.1 instead of 0.05) to determine the most significant outliers for biological validation. To visualize global trends in the dataset, we performed a 1D annotation enrichment (Benjamini–Hochberg FDR cutoff of 0.05) based on the differences in means. Significantly enriched annotations (KEGG name, GOMF name, keyword, GOCC slim name) are depicted in table (1D annotation enrichment). For biological follow-ups, we focused on proteins with highest fold change.

Labeling of glycoproteins at the cell surface and mass spectrometric analysis

The protocol was adapted from Kuhn *et al* (2012); 4.5 million neurons in a 10-cm dish labeled for 48 h with 200 nM ManNAz was washed twice with cold PBS. Afterward, 100 nM DBCO-PEG12-biotin (Click Chemistry Tools) diluted in 2 ml PBS was evenly distributed on the neurons and incubated at 4°C for 2 h. Neurons were washed twice with PBS and then lysed in 5 ml buffer (150 mM NaCl, 50 mM Tris, 2 mM EDTA, 1 % NP-40) per dish. After centrifugation at 4,000 *g*, equal protein amounts of the clarified lysate were loaded on a PolyPrep column with a streptavidin bead bed (300 μl slurry). After binding of proteins, streptavidin beads were washed three times with 10 ml PBS supplemented with 1% SDS. To elute the biotinylated glycoproteins, streptavidin beads were boiled with urea sample buffer containing 3 mM biotin.

Samples were analyzed twice using an Easy-NLC 1000 nanoflow HPLC system II (Proxeon) connected to an LTQ-Velos Orbitrap Pro (Thermo Fisher Scientific). Peptides were separated by reverse-phase chromatography using in-house-made 30-cm columns (New Objective, FS360-75-8-N-S-C30) packed with C18-AQ 2.4-μm resin (Dr Maisch GmbH, Part No. r124.aq). A 90-min gradient (5–40%) at a flow rate of 200 nl/min was used. The measurement method consisted of an initial FTMS scan recorded in profile mode with 30,000 m/z resolution, a mass range from 300 to 2,000 m/z, and a target value of 1,000,000. Subsequently, collision-induced dissociation (CID) fragmentation was performed for the 15 most intense ions with an isolation width of 2 Da in the ion trap. A target value of 10,000, enabled charge state screening, a monoisotopic precursor selection, 35% normalized collision energy, an activation time of 10 ms, wide band activation, and a dynamic exclusion list with 30-s exclusion time were applied.

Data from three independent experiments with two technical replicates were analyzed with MaxQuant suite (version 1.5.3.12) in combination with the Andromeda search algorithm as above. First search, mass recalibration, and main search of tryptic peptides were performed using a rat Uniprot database downloaded on the 21 August 2012. Two missed cleavages were allowed. Peptide as well as protein false discovery rate was set to 1%. Mass accuracy was set to 20 ppm for the first search and 5 ppm for the main search. Quantification was performed between the respective control and TDP-43-knockdown condition on the basis of unique and razor peptides. Missing values were imputed in Perseus 1.5.16 following a standard distribution. *P*-values were calculated from $\log_2$-transformed LFQ ratios using a heteroscedastic, two-sided Student's *t*-test. Proteins with a *P*-value of $P \leq 0.05$ were considered as hits. To correct for multiple hypothesis testing, the Benjamini–Hochberg post-test was applied with an adjusted false discovery rate of 0.05.

Data availability

The mass spectrometry data have been deposited to the ProteomeXchange Consortium via the PRIDE (Vizcaino *et al*, 2016) partner repository [http://www.ebi.ac.uk/pride/] with the dataset identifier PXD004756 (whole proteome) and PXD004744 (cell surface proteome).

Expanded View for this article is available online.

Author contributions

BMS and DE conceived the project and designed the experiments. BMS performed and analyzed live imaging and cell biological experiments. HH, AC, ST, DO, MM, and FS contributed to cell biological experiments. AS, DH, FM, and P-HK generated proteomics data. MHS and TA provided and analyzed brain section. SH, MP, and OB provided human neurons. CK, TK, MO, and ACL provided patient CSF samples and clinical input. BMS and DE wrote the manuscript with input from all coauthors.

Conflict of interest

The authors declare that they have no conflict of interest.

References

Adell MA, Teis D (2011) Assembly and disassembly of the ESCRT-III membrane scission complex. *FEBS Lett* 585: 3191 – 3196

Alami NH, Smith RB, Carrasco MA, Williams LA, Winborn CS, Han SS, Kiskinis E, Winborn B, Freibaum BD, Kanagaraj A, Clare AJ, Badders NM, Bilican B, Chaum E, Chandran S, Shaw CE, Eggan KC, Maniatis T, Taylor JP (2014) Axonal transport of TDP-43 mRNA granules is impaired by ALS-causing mutations. *Neuron* 81: 536 – 543

Allison JG, Das PM, Ma J, Inglis FM, Jones FE (2011) The ERBB4 intracellular domain (4ICD) regulates NRG1-induced gene expression in hippocampal neurons. *Neurosci Res* 70: 155 – 163

Brettschneider J, Mogel H, Lehmensiek V, Ahlert T, Sussmuth S, Ludolph AC, Tumani H (2008) Proteome analysis of cerebrospinal fluid in amyotrophic lateral sclerosis (ALS). *Neurochem Res* 33: 2358 – 2363

Buratti E, Romano M, Baralle FE (2013) TDP-43 high throughput screening analyses in neurodegeneration: advantages and pitfalls. *Mol Cell Neurosci* 56: 465 – 474

Cahill ME, Jones KA, Rafalovich I, Xie Z, Barros CS, Muller U, Penzes P (2012) Control of interneuron dendritic growth through NRG1/erbB4-mediated kalirin-7 disinhibition. *Mol Psychiatry* 17: 99 – 107

Choudhury A, Dominguez M, Puri V, Sharma DK, Narita K, Wheatley CL, Marks DL, Pagano RE (2002) Rab proteins mediate Golgi transport of caveola-internalized glycosphingolipids and correct lipid trafficking in Niemann-Pick C cells. *J Clin Invest* 109: 1541 – 1550

Cirulli ET, Lasseigne BN, Petrovski S, Sapp PC, Dion PA, Leblond CS, Couthouis J, Lu YF, Wang Q, Krueger BJ, Ren Z, Keebler J, Han Y, Levy SE, Boone BE, Wimbish JR, Waite LL, Jones AL, Carulli JP, Day-Williams AG *et al* (2015) Exome sequencing in amyotrophic lateral sclerosis identifies risk genes and pathways. *Science* 347: 1436 – 1441

Collins MA, An J, Hood BL, Conrads TP, Bowser RP (2015) Label-Free LC-MS/MS Proteomic Analysis of Cerebrospinal Fluid Identifies Protein/Pathway Alterations and Candidate Biomarkers for Amyotrophic Lateral Sclerosis. *J Proteome Res* 14: 4486 – 4501

Cooper MA, Koleske AJ (2014) Ablation of ErbB4 from excitatory neurons leads to reduced dendritic spine density in mouse prefrontal cortex. *J Comp Neurol* 522: 3351 – 3362

Cox J, Mann M (2008) MaxQuant enables high peptide identification rates, individualized p.p.b.-range mass accuracies and proteome-wide protein quantification. *Nat Biotechnol* 26: 1367 – 1372

Cox J, Neuhauser N, Michalski A, Scheltema RA, Olsen JV, Mann M (2011) Andromeda: a peptide search engine integrated into the MaxQuant environment. *J Proteome Res* 10: 1794 – 1805

Cox J, Hein MY, Luber CA, Paron I, Nagaraj N, Mann M (2014) Accurate proteome-wide label-free quantification by delayed normalization and maximal peptide ratio extraction, termed MaxLFQ. *Mol Cell Proteomics* 13: 2513 – 2526

Davidson YS, Raby S, Foulds PG, Robinson A, Thompson JC, Sikkink S, Yusuf I, Amin H, DuPlessis D, Troakes C, Al-Sarraj S, Sloan C, Esiri MM, Prasher VP, Allsop D, Neary D, Pickering-Brown SM, Snowden JS, Mann DM (2011) TDP-43 pathological changes in early onset familial and sporadic Alzheimer's disease, late onset Alzheimer's disease and Down's syndrome: association with age, hippocampal sclerosis and clinical phenotype. *Acta Neuropathol* 122: 703 – 713

Du X, Kazim AS, Dawes IW, Brown AJ, Yang H (2013) The AAA ATPase VPS4/SKD1 regulates endosomal cholesterol trafficking independently of ESCRT-III. *Traffic* 14: 107 – 119

Ebens A, Brose K, Leonardo ED, Hanson MG Jr, Bladt F, Birchmeier C, Barres BA, Tessier-Lavigne M (1996) Hepatocyte growth factor/scatter factor is an axonal chemoattractant and a neurotrophic factor for spinal motor neurons. *Neuron* 17: 1157 – 1172

Esteves da Silva M, Adrian M, Schatzle P, Lipka J, Watanabe T, Cho S, Futai K, Wierenga CJ, Kapitein LC, Hoogenraad CC (2015) Positioning of AMPA Receptor-Containing Endosomes Regulates Synapse Architecture. *Cell Rep* 13: 933 – 943

Ferrari R, Kapogiannis D, Huey ED, Momeni P (2011) FTD and ALS: a tale of two diseases. *Curr Alzheimer Res* 8: 273 – 294

Filimonenko M, Stuffers S, Raiborg C, Yamamoto A, Malerod L, Fisher EM, Isaacs A, Brech A, Stenmark H, Simonsen A (2007) Functional multivesicular bodies are required for autophagic clearance of protein aggregates associated with neurodegenerative disease. *J Cell Biol* 179: 485 – 500

Freischmidt A, Wieland T, Richter B, Ruf W, Schaeffer V, Muller K, Marroquin N, Nordin F, Hubers A, Weydt P, Pinto S, Press R, Millecamps S, Molko N, Bernard E, Desnuelle C, Soriani MH, Dorst J, Graf E, Nordstrom U *et al* (2015) Haploinsufficiency of TBK1 causes familial ALS and fronto-temporal dementia. *Nat Neurosci* 18: 631 – 636

Gendron TF, Petrucelli L (2011) Rodent models of TDP-43 proteinopathy: investigating the mechanisms of TDP-43-mediated neurodegeneration. *J Mol Neurosci* 45: 486 – 499

Gerecke KM, Wyss JM, Carroll SL (2004) Neuregulin-1beta induces neurite extension and arborization in cultured hippocampal neurons. *Mol Cell Neurosci* 27: 379 – 393

Geser F, Martinez-Lage M, Kwong LK, Lee VM, Trojanowski JQ (2009a) Amyotrophic lateral sclerosis, frontotemporal dementia and beyond: the TDP-43 diseases. *J Neurol* 256: 1205 – 1214

Geser F, Martinez-Lage M, Robinson J, Uryu K, Neumann M, Brandmeir NJ, Xie SX, Kwong LK, Elman L, McCluskey L, Clark CM, Malunda J, Miller BL, Zimmerman EA, Qian J, Van Deerlin V, Grossman M, Lee VM, Trojanowski JQ (2009b) Clinical and pathological continuum of multisystem TDP-43 proteinopathies. *Arch Neurol* 66: 180 – 189

Goh LK, Sorkin A (2013) Endocytosis of receptor tyrosine kinases. *Cold Spring Harb Perspect Biol* 5: a017459

Gotzl JK, Mori K, Damme M, Fellerer K, Tahirovic S, Kleinberger G, Janssens J, van der Zee J, Lang CM, Kremmer E, Martin JJ, Engelborghs S, Kretzschmar HA, Arzberger T, Van Broeckhoven C, Haass C, Capell A (2014) Common pathobiochemical hallmarks of progranulin-associated frontotemporal lobar degeneration and neuronal ceroid lipofuscinosis. *Acta Neuropathol* 127: 845 – 860

Han JH, Ryu HH, Jun MH, Jang DJ, Lee JA (2012) The functional analysis of the CHMP2B missense mutation associated with neurodegenerative diseases in the endo-lysosomal pathway. *Biochem Biophys Res Commun* 421: 544 – 549

Hornburg D, Drepper C, Butter F, Meissner F, Sendtner M, Mann M (2014) Deep proteomic evaluation of primary and cell line motoneuron disease models delineates major differences in neuronal characteristics. *Mol Cell Proteomics* 13: 3410 – 3420

Johnson BS, Snead D, Lee JJ, McCaffery JM, Shorter J, Gitler AD (2009) TDP-43 is intrinsically aggregation-prone, and amyotrophic lateral sclerosis-linked mutations accelerate aggregation and increase toxicity. *J Biol Chem* 284: 20329 – 20339

Jouvenet N (2012) Dynamics of ESCRT proteins. *Cell Mol Life Sci* 69: 4121 – 4133

Kabashi E, Valdmanis PN, Dion P, Spiegelman D, McConkey BJ, Vande Velde C, Bouchard JP, Lacomblez L, Pochigaeva K, Salachas F, Pradat PF, Camu W, Meininger V, Dupre N, Rouleau GA (2008) TARDBP mutations in individuals with sporadic and familial amyotrophic lateral sclerosis. *Nat Genet* 40: 572 – 574

Kaech S, Banker G (2006) Culturing hippocampal neurons. *Nat Protoc* 1: 2406–2415

Kato S, Funakoshi H, Nakamura T, Kato M, Nakano I, Hirano A, Ohama E (2003) Expression of hepatocyte growth factor and c-Met in the anterior horn cells of the spinal cord in the patients with amyotrophic lateral sclerosis (ALS): immunohistochemical studies on sporadic ALS and familial ALS with superoxide dismutase 1 gene mutation. *Acta Neuropathol* 106: 112–120

Koch P, Opitz T, Steinbeck JA, Ladewig J, Brustle O (2009) A rosette-type, self-renewing human ES cell-derived neural stem cell with potential for in vitro instruction and synaptic integration. *Proc Natl Acad Sci USA* 106: 3225–3230

Krivosheya D, Tapia L, Levinson JN, Huang K, Kang Y, Hines R, Ting AK, Craig AM, Mei L, Bamji SX, El-Husseini A (2008) ErbB4-neuregulin signaling modulates synapse development and dendritic arborization through distinct mechanisms. *J Biol Chem* 283: 32944–32956

Kuhn PH, Koroniak K, Hogl S, Colombo A, Zeitschel U, Willem M, Volbracht C, Schepers U, Imhof A, Hoffmeister A, Haass C, Rossner S, Brase S, Lichtenthaler SF (2012) Secretome protein enrichment identifies physiological BACE1 protease substrates in neurons. *EMBO J* 31: 3157–3168

Lane RF, St George-Hyslop P, Hempstead BL, Small SA, Strittmatter SM, Gandy S (2012) Vps10 family proteins and the retromer complex in aging-related neurodegeneration and diabetes. *J Neurosci* 32: 14080–14086

Lang CM, Fellerer K, Schwenk BM, Kuhn PH, Kremmer E, Edbauer D, Capell A, Haass C (2012) Membrane orientation and subcellular localization of transmembrane protein 106B (TMEM106B), a major risk factor for frontotemporal lobar degeneration. *J Biol Chem* 287: 19355–19365

Lee HH, Elia N, Ghirlando R, Lippincott-Schwartz J, Hurley JH (2008) Midbody targeting of the ESCRT machinery by a noncanonical coiled coil in CEP55. *Science* 322: 576–580

Li B, Woo RS, Mei L, Malinow R (2007) The neuregulin-1 receptor erbB4 controls glutamatergic synapse maturation and plasticity. *Neuron* 54: 583–597

Ling SC, Polymenidou M, Cleveland DW (2013) Converging mechanisms in ALS and FTD: disrupted RNA and protein homeostasis. *Neuron* 79: 416–438

Lu Y, Ferris J, Gao FB (2009) Frontotemporal dementia and amyotrophic lateral sclerosis-associated disease protein TDP-43 promotes dendritic branching. *Mol Brain* 2: 30

Mackenzie IR, Rademakers R, Neumann M (2010) TDP-43 and FUS in amyotrophic lateral sclerosis and frontotemporal dementia. *Lancet Neurol* 9: 995–1007

Mackenzie IR, Arzberger T, Kremmer E, Troost D, Lorenzl S, Mori K, Weng SM, Haass C, Kretzschmar HA, Edbauer D, Neumann M (2013) Dipeptide repeat protein pathology in C9ORF72 mutation cases: clinico-pathological correlations. *Acta Neuropathol* 126: 859–879

Maxfield FR, McGraw TE (2004) Endocytic recycling. *Nat Rev Mol Cell Biol* 5: 121–132

McCloy RA, Rogers S, Caldon CE, Lorca T, Castro A, Burgess A (2014) Partial inhibition of Cdk1 in G 2 phase overrides the SAC and decouples mitotic events. *Cell Cycle* 13: 1400–1412

Michalski A, Damoc E, Hauschild JP, Lange O, Wieghaus A, Makarov A, Nagaraj N, Cox J, Mann M, Horning S (2011) Mass spectrometry-based proteomics using Q Exactive, a high-performance benchtop quadrupole Orbitrap mass spectrometer. *Mol Cell Proteomics* 10: M111.011015

Moreau K, Ravikumar B, Puri C, Rubinsztein DC (2012) Arf6 promotes autophagosome formation via effects on phosphatidylinositol 4,5-bisphosphate and phospholipase D. *J Cell Biol* 196: 483–496

Nadjar Y, Gordon P, Corcia P, Bensimon G, Pieroni L, Meininger V, Salachas F (2012) Elevated serum ferritin is associated with reduced survival in amyotrophic lateral sclerosis. *PLoS ONE* 7: e45034

Orozco D, Tahirovic S, Rentzsch K, Schwenk BM, Haass C, Edbauer D (2012) Loss of fused in sarcoma (FUS) promotes pathological Tau splicing. *EMBO Rep* 13: 759–764

Ou SH, Wu F, Harrich D, Garcia-Martinez LF, Gaynor RB (1995) Cloning and characterization of a novel cellular protein, TDP-43, that binds to human immunodeficiency virus type 1 TAR DNA sequence motifs. *J Virol* 69: 3584–3596

Passafaro M, Piech V, Sheng M (2001) Subunit-specific temporal and spatial patterns of AMPA receptor exocytosis in hippocampal neurons. *Nat Neurosci* 4: 917–926

Polymenidou M, Lagier-Tourenne C, Hutt KR, Huelga SC, Moran J, Liang TY, Ling SC, Sun E, Wancewicz E, Mazur C, Kordasiewicz H, Sedaghat Y, Donohue JP, Shiue L, Bennett CF, Yeo GW, Cleveland DW (2011) Long pre-mRNA depletion and RNA missplicing contribute to neuronal vulnerability from loss of TDP-43. *Nat Neurosci* 14: 459–468

Prickett TD, Agrawal NS, Wei X, Yates KE, Lin JC, Wunderlich JR, Cronin JC, Cruz P, Rosenberg SA, Samuels Y (2009) Analysis of the tyrosine kinome in melanoma reveals recurrent mutations in ERBB4. *Nat Genet* 41: 1127–1132

Schwartz SL, Cao C, Pylypenko O, Rak A, Wandinger-Ness A (2007) Rab GTPases at a glance. *J Cell Sci* 120: 3905–3910

Schwenk BM, Lang CM, Hogl S, Tahirovic S, Orozco D, Rentzsch K, Lichtenthaler SF, Hoogenraad CC, Capell A, Haass C, Edbauer D (2014) The FTLD risk factor TMEM106B and MAP6 control dendritic trafficking of lysosomes. *EMBO J* 33: 450–467

Shirasaki R, Lewcock JW, Lettieri K, Pfaff SL (2006) FGF as a target-derived chemoattractant for developing motor axons genetically programmed by the LIM code. *Neuron* 50: 841–853

Skibinski G, Parkinson NJ, Brown JM, Chakrabarti L, Lloyd SL, Hummerich H, Nielsen JE, Hodges JR, Spillantini MG, Thusgaard T, Brandner S, Brun A, Rossor MN, Gade A, Johannsen P, Sorensen SA, Gydesen S, Fisher EM, Collinge J (2005) Mutations in the endosomal ESCRTIII-complex subunit CHMP2B in frontotemporal dementia. *Nat Genet* 37: 806–808

Smith KR, Damiano J, Franceschetti S, Carpenter S, Canafoglia L, Morbin M, Rossi G, Pareyson D, Mole SE, Staropoli JF, Sims KB, Lewis J, Lin WL, Dickson DW, Dahl HH, Bahlo M, Berkovic SF (2012) Strikingly different clinicopathological phenotypes determined by progranulin-mutation dosage. *Am J Hum Genet* 90: 1102–1107

Sonnichsen B, De Renzis S, Nielsen E, Rietdorf J, Zerial M (2000) Distinct membrane domains on endosomes in the recycling pathway visualized by multicolor imaging of Rab4, Rab5, and Rab11. *J Cell Biol* 149: 901–914

Sreedharan J, Blair IP, Tripathi VB, Hu X, Vance C, Rogelj B, Ackerley S, Durnall JC, Williams KL, Buratti E, Baralle F, de Belleroche J, Mitchell JD, Leigh PN, Al-Chalabi A, Miller CC, Nicholson G, Shaw CE (2008) TDP-43 mutations in familial and sporadic amyotrophic lateral sclerosis. *Science* 319: 1668–1672

Stagi M, Klein ZA, Gould TJ, Bewersdorf J, Strittmatter SM (2014) Lysosome size, motility and stress response regulated by fronto-temporal dementia modifier TMEM106B. *Mol Cell Neurosci* 61: 226–240

Stuchell-Brereton MD, Skalicky JJ, Kieffer C, Karren MA, Ghaffarian S, Sundquist WI (2007) ESCRT-III recognition by VPS4 ATPases. *Nature* 449: 740–744

Takahashi Y, Fukuda Y, Yoshimura J, Toyoda A, Kurppa K, Moritoyo H, Belzil VV, Dion PA, Higasa K, Doi K, Ishiura H, Mitsui J, Date H, Ahsan B, Matsukawa T, Ichikawa Y, Moritoyo T, Ikoma M, Hashimoto T, Kimura F

et al (2013) ERBB4 mutations that disrupt the neuregulin-ErbB4 pathway cause amyotrophic lateral sclerosis type 19. *Am J Hum Genet* 93: 900−905

Tashiro Y, Urushitani M, Inoue H, Koike M, Uchiyama Y, Komatsu M, Tanaka K, Yamazaki M, Abe M, Misawa H, Sakimura K, Ito H, Takahashi R (2012) Motor neuron-specific disruption of proteasomes, but not autophagy, replicates amyotrophic lateral sclerosis. *J Biol Chem* 287: 42984−42994

Teng YD, Mocchetti I, Taveira-DaSilva AM, Gillis RA, Wrathall JR (1999) Basic fibroblast growth factor increases long-term survival of spinal motor neurons and improves respiratory function after experimental spinal cord injury. *J Neurosci* 19: 7037−7047

Tollervey JR, Curk T, Rogelj B, Briese M, Cereda M, Kayikci M, Konig J, Hortobagyi T, Nishimura AL, Zupunski V, Patani R, Chandran S, Rot G, Zupan B, Shaw CE, Ule J (2011) Characterizing the RNA targets and position-dependent splicing regulation by TDP-43. *Nat Neurosci* 14: 452−458

Tu C, Ahmad G, Mohapatra B, Bhattacharyya S, Ortega-Cava CF, Chung BM, Wagner KU, Raja SM, Naramura M, Band V, Band H (2011) ESCRT proteins: Double-edged regulators of cellular signaling. *Bioarchitecture* 1: 45−48

Tusher VG, Tibshirani R, Chu G (2001) Significance analysis of microarrays applied to the ionizing radiation response. *Proc Natl Acad Sci USA* 98: 5116−5121

Urwin H, Authier A, Nielsen JE, Metcalf D, Powell C, Froud K, Malcolm DS, Holm I, Johannsen P, Brown J, Fisher EM, van der Zee J, Bruyland M, Van Broeckhoven C, Collinge J, Brandner S, Futter C, Isaacs AM (2010) Disruption of endocytic trafficking in frontotemporal dementia with CHMP2B mutations. *Hum Mol Genet* 19: 2228−2238

Vizcaino JA, Csordas A, del-Toro N, Dianes JA, Griss J, Lavidas I, Mayer G, Perez-Riverol Y, Reisinger F, Ternent T, Xu QW, Wang R, Hermjakob H (2016) 2016 update of the PRIDE database and its related tools. *Nucleic Acids Res* 44: D447−D456

Walker AK, Spiller KJ, Ge G, Zheng A, Xu Y, Zhou M, Tripathy K, Kwong LK, Trojanowski JQ, Lee VM (2015) Functional recovery in new mouse models of ALS/FTLD after clearance of pathological cytoplasmic TDP-43. *Acta Neuropathol* 130: 643−660

Wu LS, Cheng WC, Shen CK (2012) Targeted depletion of TDP-43 expression in the spinal cord motor neurons leads to the development of amyotrophic lateral sclerosis-like phenotypes in mice. *J Biol Chem* 287: 27335−27344

Xia Q, Wang H, Hao Z, Fu C, Hu Q, Gao F, Ren H, Chen D, Han J, Ying Z, Wang G (2015) TDP-43 loss of function increases TFEB activity and blocks autophagosome-lysosome fusion. *EMBO J* 35: 121−142

Yoshimori T, Yamagata F, Yamamoto A, Mizushima N, Kabeya Y, Nara A, Miwako I, Ohashi M, Ohsumi M, Ohsumi Y (2000) The mouse SKD1, a homologue of yeast Vps4p, is required for normal endosomal trafficking and morphology in mammalian cells. *Mol Biol Cell* 11: 747−763